

## Research Article

## High temperature pure carbon nanoparticle formation: Validation of AIREBO and ReaxFF reactive molecular dynamics

Nikita Orekhov <sup>a, b, d, \*</sup>, Gulnaz Ostroumova <sup>a, b, \*\*</sup>, Vladimir Stegailov <sup>a, b, c</sup><sup>a</sup> Joint Institute for High Temperatures of the Russian Academy of Sciences, 13 Izhorskaya Bd 2, Moscow, Russian Federation<sup>b</sup> Moscow Institute of Physics and Technology, 9 Institutskiy per., Dolgoprudny, Moscow Region, Russian Federation<sup>c</sup> National Research University Higher School of Economics, 20 Myasnitskaya Str., Moscow, Russian Federation<sup>d</sup> Bauman Moscow State Technical University, 5 2nd Baumanskaya Str., Moscow, Russian Federation

## ARTICLE INFO

## Article history:

Received 1 April 2020

Received in revised form

28 July 2020

Accepted 5 August 2020

Available online 25 August 2020

## Keywords:

Bond order potentials

Nucleation

Condensation

Graphitization

Fullerenes

DFTB

DFT

## ABSTRACT

Molecular dynamics with reactive interatomic potentials is the only computationally feasible approach for modeling at the atomistic level the formation of carbon nanoparticles from gas state. Such models require thousands of atoms and millions of time steps that is beyond the current capabilities of first principles electronic structure calculations. A continuously growing variety of available reactive interatomic potentials for carbon requires their careful validation for a particular molecular system and pressure-temperature conditions. In this work we consider a generic example process of carbon nanoparticle formation at cooling of the gas phase and compare different AIREBO and ReaxFF reactive models. Three main processes of clusterization, change of hybridization and graphitization are analysed and used for comparison of potentials. *Ab initio* density functional theory and parameterized density functional tight-binding calculations together with experimental data available are used for validation of the reactive models considered. We highlight the detected problems of some well-known reactive potentials and conclude with three models that can be selected as the best options for molecular dynamics simulations of pure carbon nanoparticle formation.

© 2020 Elsevier Ltd. All rights reserved.

## 1. Introduction

Formation of carbon nanostructures (fullerenes, graphenes, nanotubes, nanofibers and etc.) from homogeneous gas (or plasma) phase is an important technological process, and its optimization requires detailed knowledge of the corresponding atomistic mechanisms [1–6]. Various methods were used to shed light on the early stages of nucleation processes in gas-phase carbonaceous systems. And for more than twenty years, since the development of the first reactive interatomic potentials for carbon [7–9], molecular dynamics (MD) remains one of the most commonly used tools for numerical investigation in this field. The carbon nanostructures nucleation can be studied in the framework of thermodynamics [10,11]. But simulations at the atomistic level can provide both

thermophysical properties and detailed information about transport properties (e.g. see Ref. [12,13]). MD has already covered such fields of interest as fullerenes [14], carbon nanotubes (CNT) [15] and graphene [16] bottom-up fabrication, high-temperature soot formation [17,18], hydrocarbon fuel cracking [19]. Being the basis of the whole organic chemistry, carbon reveals the complex chemical behavior including mixed hybridization and  $\pi$ -conjugation and therefore requires sophisticated analytical models of interatomic potentials for MD. The variety of such models grows continuously giving rise to inner contradictoriness between different potential models or even between different parameter sets within one model or a force field [20]. Predictions on the density of liquid carbon at  $T > 5000$  K vary within more than 50% depending on the particular MD potential [21]. Recently, it has been shown that modern carbon interatomic potentials reproduce the structure of the amorphous carbon with an enormous divergence in terms of atom hybridization and level of graphitization [22]. In the later extension of that study [23], authors covered a wider set of models and demonstrated that no two potentials predicted the same structural properties for dense non-crystalline carbon phases. All of the above mentioned problems in the field of reactive molecular dynamics

\* Corresponding author. Moscow Institute of Physics and Technology, 9 Institutskiy per., Dolgoprudny, Moscow Region, Russian Federation.

\*\* Corresponding author. Joint Institute for High Temperatures of the Russian Academy of Sciences, 13 Izhorskaya Bd 2, Moscow, Russian Federation.

E-mail addresses: [nikita.orekhov@phystech.edu](mailto:nikita.orekhov@phystech.edu) (N. Orekhov), [g.gulnaz@phystech.edu](mailto:g.gulnaz@phystech.edu) (G. Ostroumova), [stegailov.vv@mpt.ru](mailto:stegailov.vv@mpt.ru) (V. Stegailov).

highlight that decisions on the preference of one of carbon potentials over another requires preliminary validation in each particular case. While authors of [23] performed tests for the condensed carbon phases with the densities from 1.5 to 3 g/cc, we focus on the structural transition appeared at the lower densities and extend our previous study of the carbon nanoparticles formation from the gas phase [24]. In this paper we compare the Adaptive Intermolecular Reactive Empirical Bond Order (AIREBO) potential [25] and several Reactive Force Field (ReaxFF [26]) parameterizations; these models are among the most widely used for reactive MD studies of carbon systems and are usually considered as viable alternatives to costly quantum mechanical simulations [27].

Despite there is a rapidly growing number of studies based on reactive MD, there are still very limited information on the comparison and validation of different reactive models [20–23].

## 2. Reactive models

In this work, we examine only carbon reactive potentials with the long-range (van der Waals) terms, which are important for a proper description of interparticle interactions in gaseous phases. Therefore we do not discuss here such popular models as Stillinger-Weber [7], Brenner [9], Tersoff [8], EDIP [28] or GAP [29,30]. Also we do not consider Long-range Carbon Bond-Order Potential (LCBOP) [31] since its first version available in LAMMPS is a preliminary version (e.g. it has no torsional term). As far as we know, the latest version with added torsional energy and improved bond dissociation description LCBOP-II [32,33] is not available for MD calculations.

The reactive nature of both AIREBO and ReaxFF takes into account the breaking and the formation of covalent bonds. The fundamental assumption of these potentials is the concept of bond-order (BO): the properties of the covalent bond created by two atoms depend not only on their types and interatomic distance but also on the local chemical environment. Two neighboring carbon atoms interact with each other differently if they are within polyyne, graphite, or diamond. This is due to the fact that atoms in these three materials have different bond orders that are associated with the  $sp$ ,  $sp^2$  and  $sp^3$  hybridizations. The concept of BO dependent potentials in MD originates in the works of Tersoff and Pettifor [8,34–36].

Modern bond-order potentials are becoming more and more sophisticated in terms of their functional form, which is the result of the long history of step-by-step development through several decades. The current situation can be illustrated by the sizes of the parameter sets used in each model. For pure carbon systems there are more than 60 major parameters in AIREBO and 39 parameters in ReaxFF. In general, one cannot predict *a priori* how an alteration of some particular parameter from one set influences the physical properties of the modeled system. Retrospectively, this statement can be illustrated by the conclusions in Ref. [37] where an intriguing liquid-liquid phase transition observed in carbon appeared to be a non-physical effect due to the overestimation of torsional barriers in the REBO potential [9,38]. The high sensitivity of the physical properties of carbon systems on the parameterization of an empirical MD potential has been also demonstrated in a recent study [39] where the variation of individual parameters of AIREBO within less than one percent has been shown to cause the 66% change in the mechanical properties of graphene.

### 2.1. AIREBO

AIREBO has been successfully applied to model a wide variety of high-temperature processes in carbon systems, including such phenomena as possible liquid-liquid phase transition in carbon

[27], fullerene and graphene formation [16], graphite [40,41] and graphene [42] melting. It is based on the Brenner's reactive empirical bond-order potential REBO [9,38,43] and additionally takes into account torsion and long-range nonbonded interactions. The total potential energy is represented as

$$E = \frac{1}{2} \sum_i \sum_{i \neq j} \left[ E_{ij}^{\text{REBO}} + E_{ij}^{\text{LJ}} + \sum_{k \neq i, j, l \neq i, j, k} E_{ijkl}^{\text{tors}} \right]. \quad (1)$$

$E_{ij}^{\text{REBO}}$  consists of the repulsive and attractive terms and depends on the bond order  $b_{ij}$  between two atoms  $i$  and  $j$ :

$$E_{ij}^{\text{REBO}} = V_{ij}^R(r_{ij}) + b_{ij} V_{ij}^A(r_{ij}). \quad (2)$$

The Lennard-Jones potential  $E_{ij}^{\text{LJ}}$  describes the long-range van der Waals interactions.

In order to prevent the rotation around single C–C bonds in hydrocarbons, AIREBO incorporates a torsional component  $E_{ijkl}^{\text{tors}}$ . It is parameterized in agreement with the experimental values of the torsional barriers in propane and butane, which are on the order of 1–4 kcal/mol.  $E_{\text{tors}}$  is added to AIREBO in order to improve the description of the large hydrocarbon systems, but it is not obvious whether it should be used in simulations of carbon-rich nanoparticles. In the original paper [25] it is mentioned that the inclusion of this barrier does not alter the properties of the bulk diamond and should not significantly affect the properties of other solid carbon systems due to the low value of  $E_{\text{tors}}$  in comparison with the typical energies of covalent C–C bonds. Here we perform the calculations with both enabled and disabled torsional barrier. The corresponding models are referred to as AIREBO<sub>tors</sub> and AIREBO<sub>notors</sub>.

Since its release in 2000, AIREBO has obtained several extensions. A slightly different so called bond-centric approach was suggested for BO evaluation in the later modification of AIREBO [44]. Unfortunately, this modification is not implemented into any of open-source MD-packages and here we leave it out of our consideration. Another interesting modification of AIREBO called AIREBO-M [45] differs from the original version by the analytical form of nonbonded van der Waals interactions: it utilizes a Morse-like function instead of Lennard-Jones. It results in a more precise reproduction of graphite density at megabar pressures, but does not significantly influence the behavior of the low-density gas-phase carbon. Therefore any results obtained here for AIREBO could be safely applied to AIREBO-M. The current implementation of AIREBO is restricted mainly to hydrocarbons, meanwhile there is REBO-CHO [46] and other extensions are possible as well. Apart from the high-temperature applications mentioned above, both REBO and AIREBO are known for their precise description of mechanical and elastic properties of carbon nanostructures near the room temperature [47–49].

### 2.2. ReaxFF

ReaxFF is a general bond-order-dependent potential known for its ability in the describing reactive chemistry in multi-element simulations. Depending on the specific parameter set its capabilities could be extended far beyond carbonaceous systems [50–55]. A significant part of ReaxFF parameterizations was developed for modeling of the combustion kinetics in hydrocarbons [26] and catalytic effects of metals on CNT nucleation [53]. Sometimes, ReaxFF parameter sets are corrected after careful analysis of a particular reaction mechanism [56].

The potential energy in ReaxFF is divided into several partial

contributions (eq. (3)) which depend on the bond order (except for the van der Waals and Coulomb interactions):

$$E_{\text{system}} = E_{\text{bond}} + E_{\text{val}} + E_{\text{tors}} + E_{\text{vdW}} + E_{\text{Coulomb}} + E_{\text{over}} + E_{\text{specific}}, \quad (3)$$

where  $E_{\text{bond}}$  represents the covalent bond energy between atoms,  $E_{\text{val}}$  describes the interaction of atoms through valence angles,  $E_{\text{tors}}$  is the energy of the torsion interactions,  $E_{\text{vdW}}$  and  $E_{\text{Coulomb}}$  are the energies which represent the non-bonded interactions. The over-coordination term  $E_{\text{over}}$  is included in the force field to avoid unrealistically high bond order values on atoms.  $E_{\text{specific}}$  describes system specific interatomic interactions, e.g. in the conjugated system,  $C_2$  molecules, 'allene'-type molecules (other specific contributions are listed in Supplementary Materials to Ref. [51]).

The key idea of ReaxFF is also based on the bond order concept. In ReaxFF the bond order is the sum of three exponential contributions:

$$\begin{aligned} BO_{ij} = BO_{ij}^{\sigma} + BO_{ij}^{\pi} + BO_{ij}^{\pi\pi} &= \exp \left[ p_{bo,1} \cdot \left( \frac{r_{ij}}{r_{\sigma}} \right)^{p_{bo,2}} \right] + \exp \left[ p_{bo,3} \cdot \left( \frac{r_{ij}^{\pi}}{r_{\sigma}} \right)^{p_{bo,4}} \right] \\ &+ \exp \left[ p_{bo,5} \cdot \left( \frac{r_{ij}^{\pi\pi}}{r_{\sigma}} \right)^{p_{bo,6}} \right], \end{aligned} \quad (4)$$

where  $p_{bo,n}$  are the bond parameters which are different for the different types of atoms.

The first contribution ( $\sigma$  bond) is close to 1 at a distance between carbon atoms of about 1.5 Å and tends to 0 at  $r_{ij} > 2.5$  Å. The second contribution ( $\pi$  bond) is equal to 1 if  $r_{ij} < 1.2$  Å and is insignificant when  $r_{ij} >$  of 1.75 Å. The third contribution ( $\pi\pi$  bond) is equal to 1 when the distance is less than 1.0 Å, and decreases sharply to 0 at 1.4 Å.

An important difference between the ReaxFF and AIREBO models is the fact that ReaxFF uses a much longer-range exponentially decaying BO/bond distance relation, without any cutoff. In AIREBO there is a cut-off for interparticle distances for the REBO energy term and the distance for covalent interactions is limited by 2 Å.

In this work, we use several ReaxFF parameterizations. In Table 1 we present the information about AIREBO and six sets of parameters of the ReaxFF models [50–55]. The models are listed in chronological order here and below. The ReaxFF parameterizations with nickel and iron are taken because of their possible use for studying the formation of carbon nanostructures in the presence of metal catalysts. The development and possible perspectives of ReaxFF model are described in more detail in Ref. [57].

### 3. Carbon nanoparticle nucleation at fast cooling

We perform MD modeling of the atomic carbon gas cooling and, based on the analysis of the clusterization process, atom hybridization and level of graphitization, highlight the differences in a structural evolution of the systems described by different potentials. The computational cell contains 1372 atoms, which allows us to cover the realistic sizes of soot nanoparticles and giant fullerenes [78]. All reactive MD calculations are performed using LAMMPS program package<sup>1</sup> [80]. Initially, atoms are uniformly distributed over the simulation cell with the volume  $V = 70 \times 70 \times 70$  Å<sup>3</sup>. The corresponding density is equal to 0.08 g/cm<sup>3</sup>.

We model the cooling from 6000 K to 2500 K during 2.5 ns,

which gives the cooling rate of 1.4 K/ns. The time step of integration of the equations of motion is chosen as 0.05 fs since the parametric study [20] showed that high-temperature simulations require such a small time step. The temperature is controlled by the Nose-Hoover thermostat [81] in canonical NVT ensemble with the damping parameter ( $T_{\text{damp}}$  in LAMMPS) 5 fs for systems with 1372 atoms and 25 fs for systems with 216 atoms. We have checked that the variation of  $T_{\text{damp}}$  from 5 fs to 100 fs causes the variation in the clusterization temperature about 100 K. The initial temperature of the system is chosen to be 6000 K to cover all the transitions from the gas phase to a liquid-like and then to a solid-like states [82,83]. The results of the cooling procedure are averaged over 3 independent MD trajectories for each interatomic potential. The maximum standard errors of the mean at the given moment of time are 20% for cluster sizes, 3% for hybridization values and 4% for graphitization values. However, these fluctuations cause negligible changes in the corresponding transition temperatures. All MD calculations are carried out at the constant volume of the simulation box, the averaged pressure in the model along the MD trajectory stays within 0.1–1 kbar range and the variation of the averaged pressure is about 0.1 kbar [24]. Computational limitations do not allow us to perform sufficiently long simulations and examine realistic cooling rates. For example, in the arc discharge experiments the gas flow experiences sharp temperature gradients of the order of 10<sup>3</sup> K/mm [84] with the speed of the flow 10<sup>5</sup> mm/s [85], which gives a rough estimation for a typical experimental cooling rate of 10<sup>-4</sup> K/ns. Nevertheless, our 10ns-long test calculations within the same temperature range have shown that the further decrease of the cooling rate does not influence the obtained results significantly.

During the cooling from a gas phase in a quasi-equilibrium way at such densities we observe several stages of structural transformations (Fig. 1) as was discussed previously in Ref. [24]:

1. nucleation of low-density clusters consisting of polymer gel [86] of small  $C_n$  molecules,
2. densification of individual clusters into liquid-like clusters,
3. graphitization of individual clusters, formation of fullerene-like particles,
4. nanoparticle coalescence (if several carbon nanoparticles are still in the simulation box).

The structures (like the one shown on Fig. 1d) are usually referred to as giant fullerenes. They contain hundreds of atoms and subsequently shrink to much smaller spherical particles [78].

As shown throughout the paper, stages (1)–(3) are qualitatively reproduced by all the potentials considered with the exceptions for ReaxFF<sub>Niels</sub> and AIREBO<sub>tors</sub>. But quantitatively, the temperature ranges of these transitions vary significantly between different ReaxFF and AIREBO parameterizations (within more than 1000 K). Fig. 2 represents the resulting structures for all the potentials considered after the cooling of the gas phase consisted of 1372 atoms during 2.5 ns from 6000 K to 2500 K.

We do not discuss here the mechanisms of carbon nanoparticles formation which could be dominant at  $T < 2500$  K. Such cases include the low-temperature CVD synthesis and a wide range of hydrocarbon combustion processes. At  $T < 3000$  K graphitization can take place simultaneously with clusters formation: e.g. in soot nanoparticles formed from small polycyclic aromatic hydrocarbons (PAH) flakes [19], which are already mostly sp<sup>2</sup>-hybridized, passing the stage of a liquid cluster. Alternatively, at  $T = 1000 – 2000$  K the formation of fullerene nanoparticles could be driven by a top-down evolution of graphene-like flakes [87].

<sup>1</sup> The bug with energy jumps for AIREBO potential in LAMMPS, mentioned in Ref. [22], has been successfully fixed by the developers [79].

**Table 1**

The summary of the reactive potentials considered. The models are described in chronological order with the number of citations from Google Scholar as of July 2020.

Reactive model	Year	Authors	Brief description	Species	Ref.	Number of citations	Most relevant citations
AIREBO	2000	S. Stuart A. Tutein J. Harrison	Suitable for modeling of the reactive inter- and intramolecular bonding in hydrocarbons; based on REBO with the addition of the long-range and torsion terms.	C H	[25]	3242	[16,27,40,42,58]
ReaxFF <sub>Niels</sub>	2005	K. Nielson A.C.T. van Duin J. Oxaard	The carbon parameters were calculated by quantum-mechanical method (QM) using the hybrid DFT/B3LYP/6-31 g++.	C H O N S Si Pt Zr Ni Cu Co X	[50]	398	[20,59–61]
ReaxFF <sub>CHO</sub>	2008	K. Chenoweth A. van Duin W. Goddard III	Developed for the description of the hydrocarbon combustion. The constants were obtained for the initial steps of hydrocarbon combustion by the adjusting of the A. van Duin training set to DFT/B3LYP/6-311 g++ calculations.	C H O	[51]	1253	[14,20,62–65]
ReaxFF <sub>FeOCH</sub>	2010	M. Aryanpour A.C.T. van Duin J.D. Kubicki	Developed to describe iron-carbide structures. The constants for carbon are based on the ReaxFF <sub>CHO</sub> hydrocarbon combustion parameter set.	C H O Fe	[52]	142	[66–69]
ReaxFF <sub>NiCH</sub>	2010	J. Mueller A. van Duin W. Goddard III	Can describe the growth of CNT and other carbon nanostructures catalyzed on nickel surfaces. The parameters for nonperiodic clusters were taken from ReaxFF <sub>Niels</sub> . All periodic constants were fitted to DFT/PBE/PW.	C H Ni	[53]	249	[70–74]
ReaxFF <sub>C2013</sub>	2015	S. Srinivasan A. van Duin P. Ganesh	The DFT/PBE/PW constants were used to reparametrize ReaxFF <sub>CHO</sub> for graphite and diamond. In order to reproduce the chemistry of carbon condensed phase and nanoparticles (especially fullerene-related) DFT/B3LYP/6-311 g++ calculations were performed.	C	[54]	132	[18,22,60,65,75,76]
ReaxFF <sub>CHO2016</sub>	2017	C. Ashraf A. van Duin	These are the improved constants of the ReaxFF <sub>CHO</sub> for small hydrocarbons (the combining of the training sets from ReaxFF <sub>CHO</sub> and ReaxFF <sub>C2013</sub> ). The carbon parameters were taken from ReaxFF <sub>C2013</sub> .	C H O	[55]	56	[77]

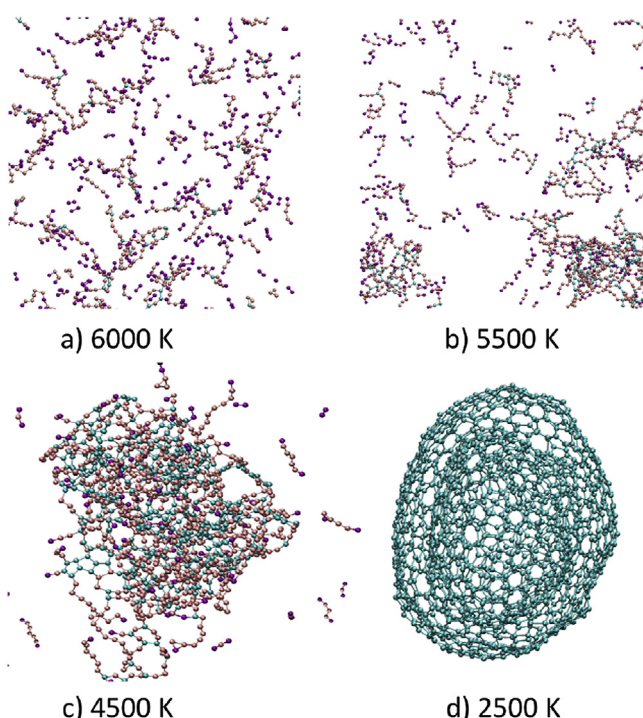


**Fig. 1.** Stages of the fullerene-like nanoparticle nucleation for ReaxFF<sub>C2013</sub>: a) 0 ns; b) 0.35 ns; c) 1 ns; d) 2.5 ns. Different colours represent different coordination numbers (purple – 1, pink – 2, cyan – 3). (A colour version of this figure can be viewed online.)

### 3.1. Clusterization

**Fig. 3** illustrates the growth of the largest cluster in the computational cell during the cooling process. A cluster here is

defined as a group of atoms, each of which is connected with at least one of the others by a covalent bond. The covalent bond cutoff radius is chosen as 1.73 Å here and below.

The cluster analysis of the products reveals a significant quantitative difference between the models considered: they show different temperatures of the start of the clusterization process from 5500 – 6000 K (AIREBO, ReaxFF<sub>C2013</sub>) to 4500 K (ReaxFF<sub>CHO</sub>, ReaxFF<sub>Niels</sub>).

For each of the discussed potentials almost all atoms unite into a single cluster at some moment. The corresponding temperature we refer to as a “clusterization temperature”. To characterise the point when the transition from the gas to the condensed phase appears, we introduce  $T_{\text{cluster}}$  as the temperature at which the maximum size of the cluster is reached. At  $T < 4000$  K the size of the largest cluster can slightly deviate from the total number of atoms (**Fig. 3**) due to the formation of onion-like structures: in some cases the inner and outer onion shells are considered as individual clusters (**Fig. 1d**).

### 3.2. Hybridization

We defined the number of atoms with particular hybridization by counting coordination numbers for all atoms. The coordination number for atoms in an ideal graphene or fullerene is equal to 3. In a linear polyyne structures it is equal to 2. The coordination number of 1 corresponds to carbon atoms with only one covalent bond, e.g. in  $\text{C}_2$  or on the ends of linear polyyne-like molecules. **Fig. 4a** demonstrates a change of the fraction of  $\text{sp}^2$ -hybridized atoms during the cooling. Here we also see significant disagreement between the considered models: AIREBO shows predominantly  $\text{sp}^2$ -hybridized structures already at  $T = 5000$  K, ReaxFF<sub>C2013</sub> and ReaxFF<sub>CHO2016</sub> demonstrate increase of  $\text{sp}^2$ -hybridized fraction in the temperature range  $T = 4300 – 4000$  K, while for ReaxFF<sub>Niels</sub> this fraction is less than 30% even at  $T = 2500$  K. The tendency of the prevalence the  $\text{sp}^2$  bonding content formed in ReaxFF<sub>C2013</sub> over

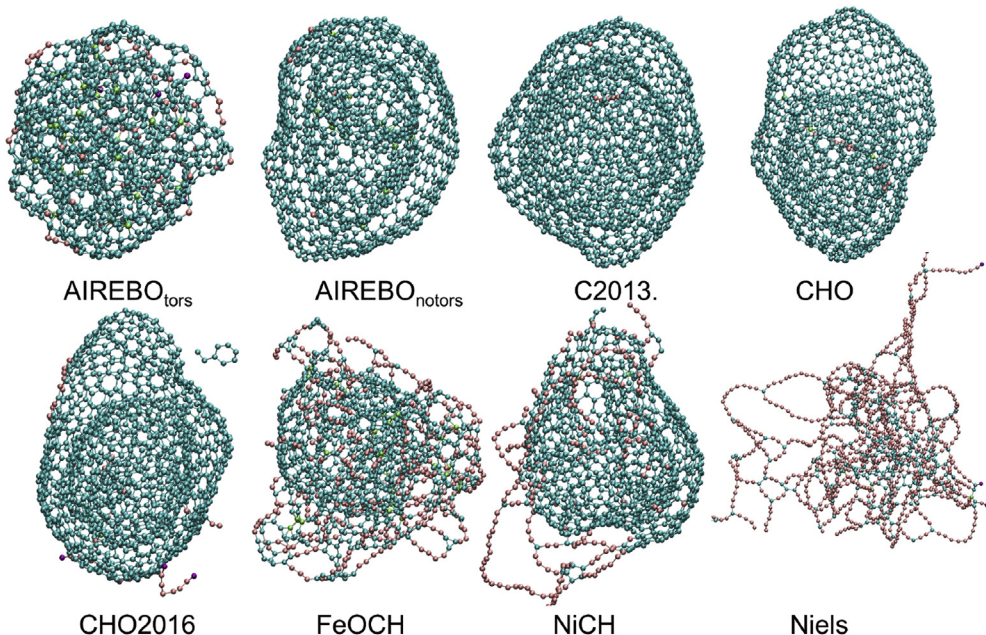


**Fig. 2.** Structures obtained by 8 models (2 AIREBO and 6 ReaxFF parameter sets) after the fast cooling from 6000 K to 2500 K. (A colour version of this figure can be viewed online.)

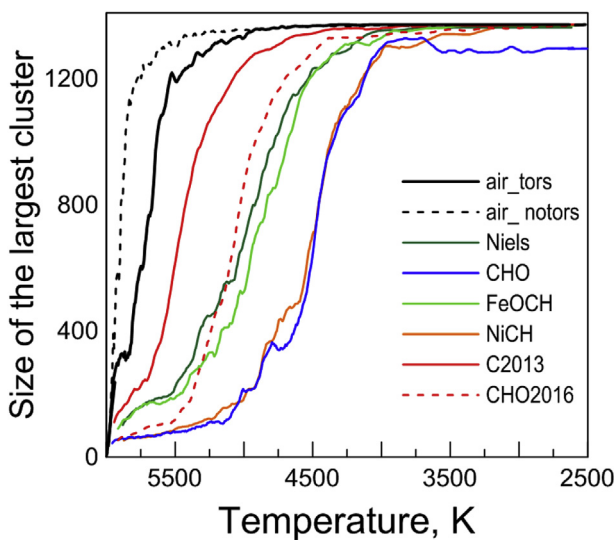


**Fig. 3.** The size of the largest cluster in the computational cell as a function of temperature during cooling from the gas phase. (A colour version of this figure can be viewed online.)

ReaxFF<sub>CHO</sub> was also detected in Ref. [65].

The temperature ranges of the hybridization change (the rise of  $sp^2$  fraction) are wider than for clusterization process (Fig. 3). From Fig. 4(a and b) it is clear that initially clusters are predominantly  $sp -$  hybridized (e.g. for ReaxFF<sub>C2013</sub> cluster is formed at 5000–5200 K while the fraction of  $sp^2 -$  hybridized atoms reaches 80% only at 4000 K).

### 3.3. Graphitization

Analysis of the coordination numbers cannot provide full information about the structure of the carbon phase:  $sp^2$  hybridized structures could be represented by an ideal fullerene or graphene as well as by some highly disordered soot nanoparticles. We conduct a

graphitization analysis described in Ref. [88] and calculate the number of pentagons, hexagons and heptagons formed by covalently connected carbon atoms as shown in Fig. 5. The high number of hexagons indicates that the structure is close to the ideal graphene.

The moment when the number of hexagons rises abruptly is referred here as the temperature of graphitization ( $T_{gr}$ ). We should notice that this definition of the graphitization temperature differs from another wide-spread definition used in experimental studies that implies the temperatures of annealing that help to reduce imperfections in  $sp^2$ -hybridized structures (e.g., see Ref. [89]).

$T_{gr}$  can be compared with the melting temperature of graphite at low pressures or with the sublimation temperature of graphene as far as all these three temperatures describe structural transition between ordered well-graphitized  $sp^2$  phase and liquid carbon.

For  $T = 2500$  K the ReaxFF parameter sets ReaxFF<sub>C2013</sub>, ReaxFF<sub>CHO2016</sub>, ReaxFF<sub>CHO</sub> demonstrate nearly the same levels of hybridization and graphitization (Figs. 4a and 6b), contrarily to ReaxFF<sub>Niels</sub>, ReaxFF<sub>FeOCH</sub> and ReaxFF<sub>NiCH</sub>. ReaxFF<sub>Niels</sub> results in non-graphitized  $sp$ -hybridized mixture of linear polymer-like chains; this problem was earlier discussed in Ref. [20] during comparative study of ReaxFF<sub>Niels</sub> and Reax<sub>CHO</sub>.

AIREBO<sub>tors</sub> demonstrates another peculiar behaviour: despite having no significant difference from the AIREBO<sub>notors</sub> in the cases of clusterization and hybridization, its hexagonal rings population is more than two times lower over the whole temperature range (Fig. 6b). Moreover it does not have any jumps of this parameter as opposed to all of the other considered potentials. It means that probably AIREBO<sub>tors</sub> does not provide proper description of the transition between disordered (liquid, amorphous) and well-graphitized crystal phases. The possible explanation of the interplay between the value of torsion barrier and the ability of the potential to describe graphitization process will be discussed in the next section.

### 4. Comparison with quantum-based methods

Reactive MD is not the only instrument applicable to model

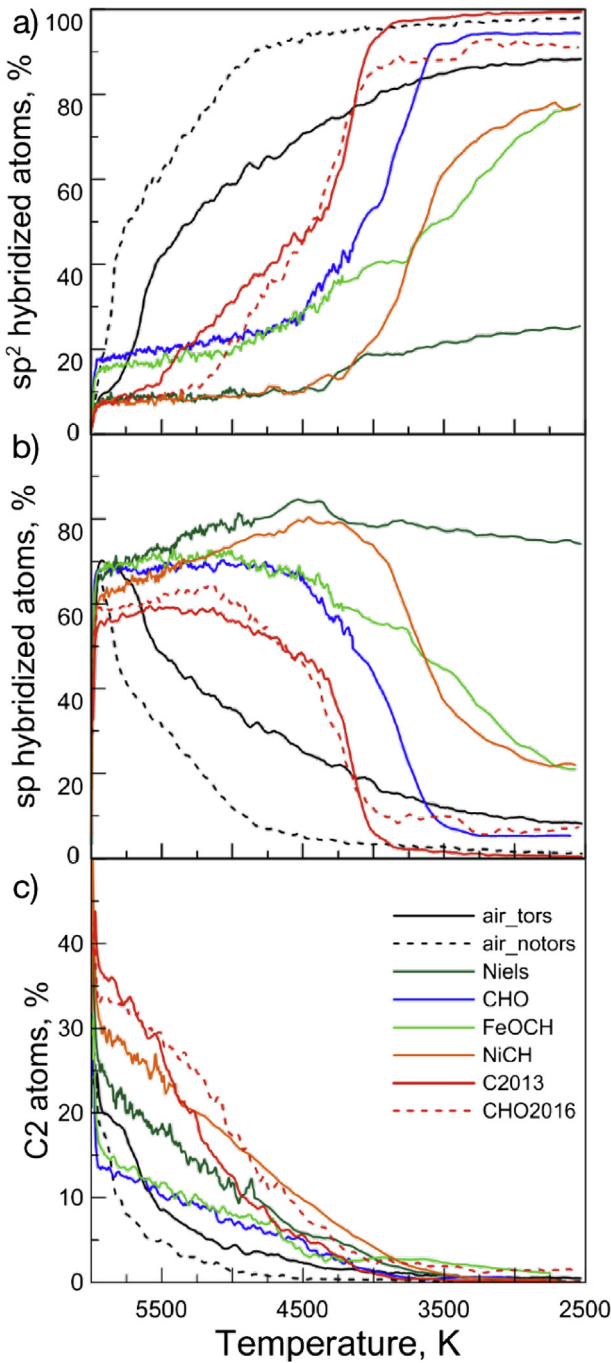


**Fig. 4.** Percentage of atoms forming C<sub>2</sub> molecules, sp- and sp<sup>2</sup>-hybridized components in the system. (A colour version of this figure can be viewed online.)

processes of carbon nanoparticles formation. Fullerene formation is simulated using quantum-based methods too [87,90,91]. The detailed review of combined quantum-classical MD simulations of carbon nanostructures is presented in Ref. [92]. The main disadvantage of quantum-based methods is caused by their high requirements on the computational time, which restrict the maximum size of the simulated system by the order of one thousand atoms that is, however, prohibitively time consuming for *ab initio* MD [93].

In this section we discuss small-scale density-functional tight-binding (DFTB) and density functional theory (DFT) calculations

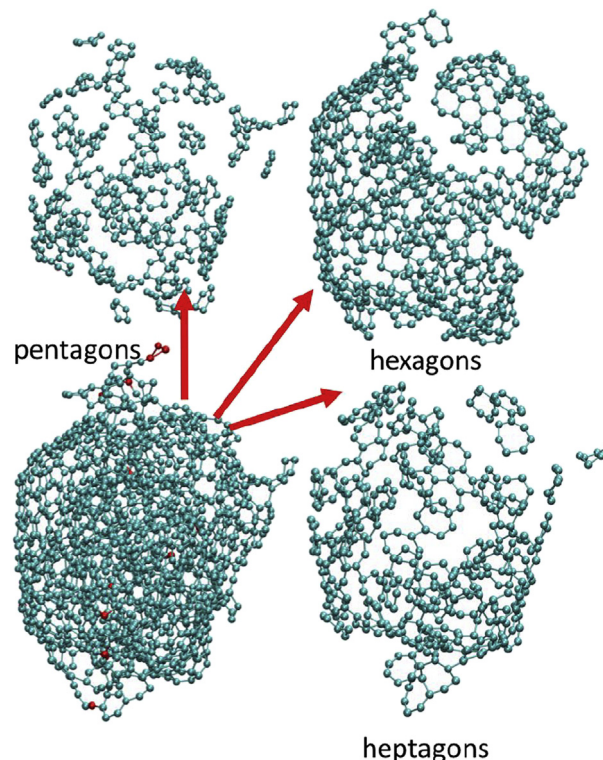


**Fig. 5.** Analysis of 5-, 6- and 7-membered rings formation for the single frame. (A colour version of this figure can be viewed online.)

to point the possible drawbacks and inaccuracies of the reactive potentials considered.

#### 4.1. Comparison with DFTB

DFTB utilizes an atomic-like basis set with Hamiltonian matrix elements and overlap integrals parameterized within density functional theory.

Here we perform calculations by employing the non-charge-consistent (NCC) DFTB [94] in which no explicit charge-charge interaction is included in the system's Hamiltonian. Such an assumption is valid for all-carbon systems [95], where effects related to charge redistribution and polarisation can be neglected. NCC DFTB (usually referred to as DFTB-1) is several times faster than the self-consistent charge variant (SCC-DFTB). Both NCC- and SCC-DFTB predict geometries of fullerene isomers close to DFT-B3LYP calculations [96]. In this work all the DFTB calculations are performed with the CP2K package [97]. For the C–C interactions we use the “pbc-0-3” parameter set [98].

For the DFTB comparison tests we build a smaller computational cell containing 216 atoms with the same density 0.08 g/cc. Since size and surface effects could play a significant role in structural evolution and final parameters of carbon nanoclusters, we also reproduce our reactive MD calculation with 216 atoms, instead of making direct comparison with the larger cell. We perform a set of independent runs at constant temperatures varied from 3000 to 6000 K and utilize the same protocol for each of MD models (i.e. for AIREBO and each ReaxFF parameter set). Each simulation lasts at least 0.5 ns which is enough to reach equilibrium structures. DFTB simulations are performed with a 0.5 fs timestep. Temperature is controlled by a Nose-Hoover thermostat in canonical NVT ensemble with the thermostat constant 25 fs. In general, AIREBO/ReaxFF clusterization, hybridization and graphitization curves for

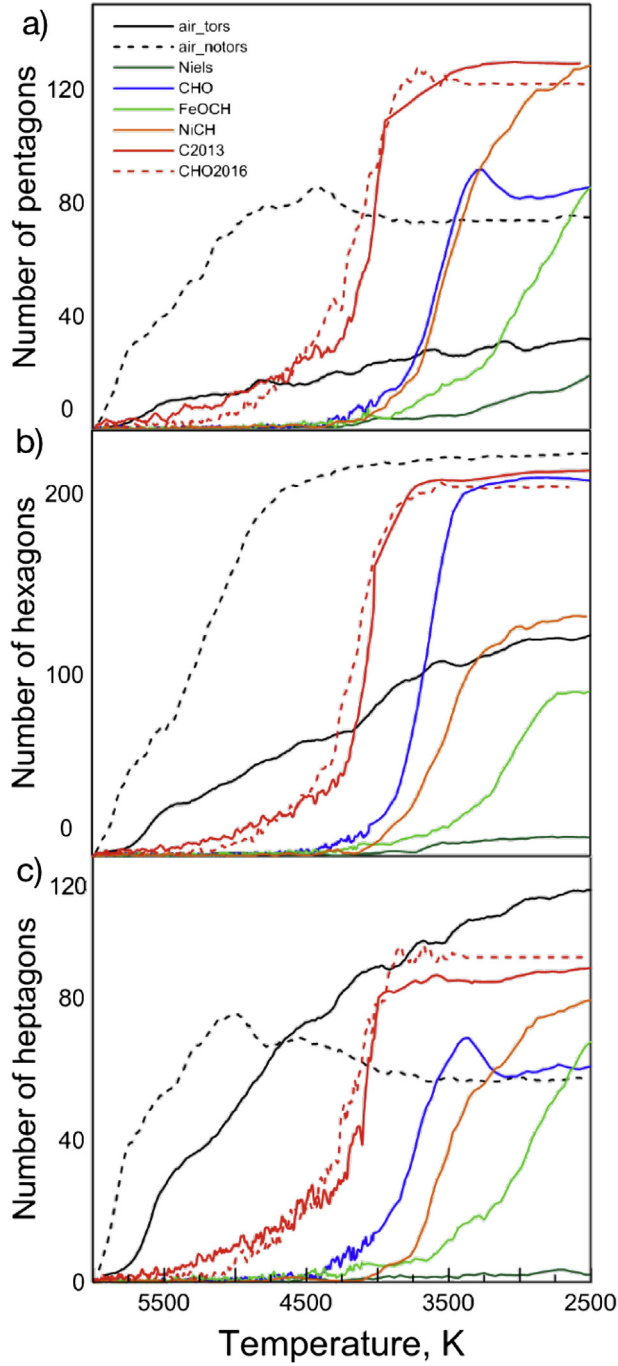


**Fig. 6.** Analysis of 5-, 6- and 7-membered ring formation for the cooling from 6000 to 2500 K during 2.5 ns

216 atoms (Fig. 7) reproduce the same trends as observed for larger system at cooling and demonstrate similarly the significant discrepancy between the potentials considered.

From Fig. 7a one can see that MD reactive potentials predict clusterization of carbon atoms at higher temperatures than DFTB. This effect is most pronounced for AIREBO<sub>notors</sub>, AIREBO<sub>tors</sub> and ReaxFF<sub>C2013</sub> potentials for which  $T_{cluster}$  exceeds the DFTB value by 500–1000 K. The significant overestimation of the graphitization temperature from DFTB is observed for AIREBO<sub>notors</sub> and ReaxFF<sub>C2013</sub>/ReaxFF<sub>CHO2016</sub>: they predict the existence of well-graphitized fullerene-like structures already at  $T = 5500$  K and

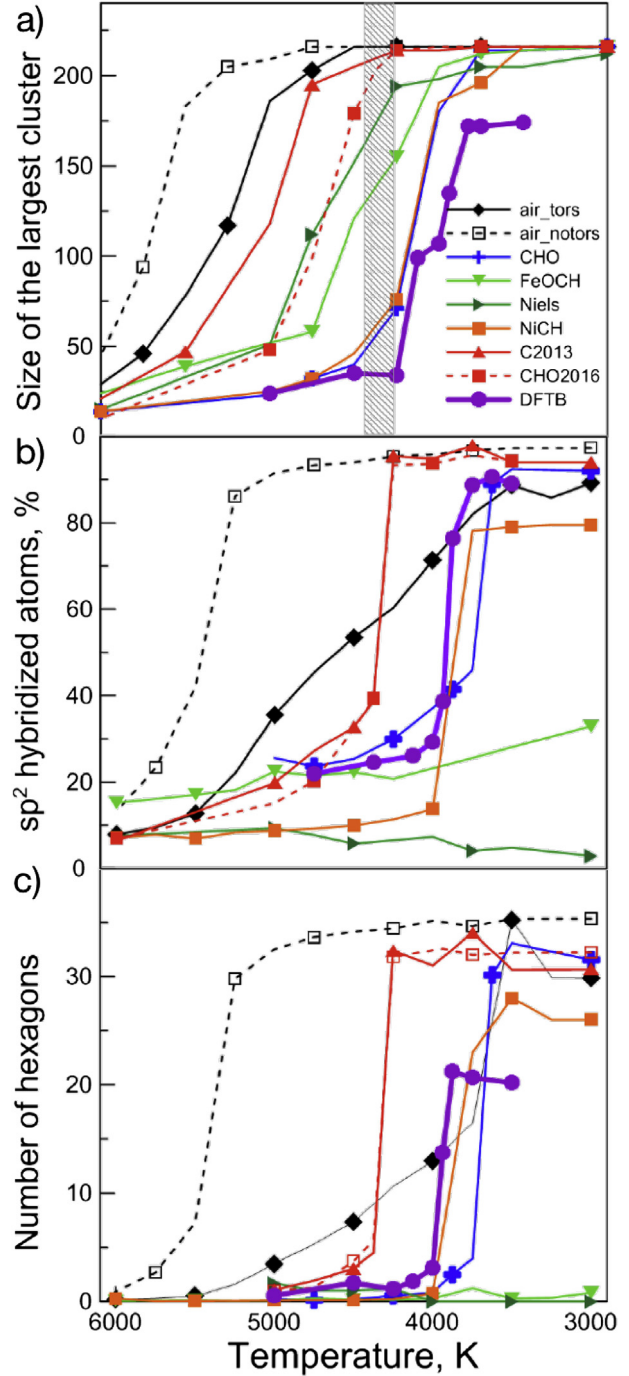


**Fig. 7.** The comparison of 8 models considered with the DFTB results on the evolution of: a) the mean size of the largest cluster in the computational cell over temperature, b) the fraction of  $sp^2$  atoms, c) the number of hexagons formed in the system. The dashed region corresponds to the highest sublimation temperatures  $T = 4250 – 4450$  K measured in Refs. [99–102]. (A colour version of this figure can be viewed online.)

$T = 4500$  K respectively while the DFTB value is  $T = 3850$  K. ReaxFF<sub>Niels</sub> and ReaxFF<sub>FeOCH</sub> are unable to reproduce the graphitization at all. The graphitization temperature is predicted by ReaxFF<sub>CHO</sub> and ReaxFF<sub>NiCH</sub> more closely to the DFTB-calculations than by other models. In DFTB simulations we do not observe complete association of all of 216 atoms into a single cluster even at  $T = 3500$  K: after the rapid formation of the fullerene cage a small part of atoms continue to stay in the form of  $C_2$  molecules and do

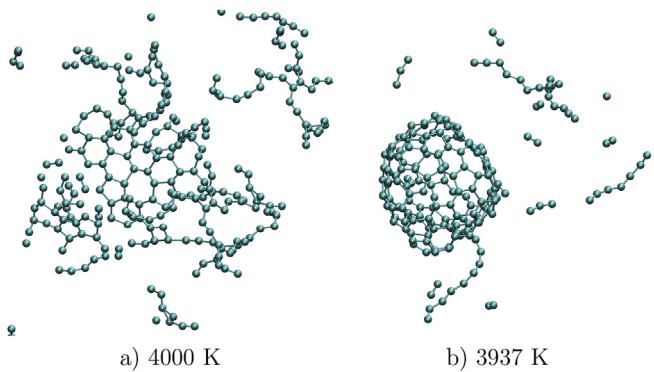


**Fig. 8.** The examples of final structures in two different DFTB constant temperature simulations. (A colour version of this figure can be viewed online.)

not merge with the main cluster, at least on the timescale of the simulation. It explains the lower numbers for the DFTB curve on Fig. 7a and, as a result, the lower number of hexagons on Fig. 7c. Nevertheless, in DFTB the carbon nanoparticle itself is well-structured and almost entirely consists of  $sp^2$ -hybridized atoms. Fig. 8 illustrates graphitization in the DFTB model.

#### 4.2. Energy barriers for collisions in gas phase

Nucleation process in gaseous phases is of collisional nature. In our case it takes place when the major part of atoms stays in  $sp$ -hybridized state forming branched polyyne-like molecules (Fig. 4b). To analyse the possible existence of repulsive barriers prohibiting the coalescence we perform calculations of the energy profile in one direction and energy landscape around the  $C_6$  molecule that is a regular hexagon consisting of  $sp$ -hybridized atoms.

Fig. 9a shows the dependence of potential energy on distance when the test atom moves perpendicular to the  $C_6$  plane. However there are many possible impact directions for the  $C_6$  hexagon and colliding carbon atom. In order to analyse them all, we calculate the potential energy landscape around a  $C_6$  ring: for the same set of interatomic potentials we move a probe atom around  $C_6$  over a cubic grid with the step 0.2 Å and compute the value of the potential energy in each point. For each potential the atomic coordinates of  $C_6$  are set to their equilibrium positions via energy minimization at  $T = 0$ K. For the further verification the same procedure is performed within DFT calculations using the TeraChem program package [103,104] with the hybrid B3LYP exchange-correlation functional [105–107] and a 6–31 g basis set.

Fig. 9b demonstrates the isosurfaces for  $E = -0.1$  and  $0.2$  eV (the attractive part and the repulsive barrier correspondingly). From the kinetic point of view the barrier covering the ring diminishes the number of collisions resulting in covalent bond formation.

In contrast to the DFT data ReaxFF<sub>Niels</sub>, ReaxFF<sub>CHO</sub> and ReaxFF<sub>FeOCH</sub> demonstrates the existence of the repulsive barrier covering the whole molecule. The energy profile for a specified direction (Fig. 9a) demonstrates that these repulsive barriers are located within 1.8–2.4 Å from the atoms of  $C_6$ , i.e. they originate from the covalent components of the potential rather than from the long-range non-bonded terms. Also Fig. 9a uncovers a narrow potential well for ReaxFF<sub>Niels</sub> and its absence for ReaxFF<sub>FeOCH</sub> and ReaxFF<sub>CHO</sub>. These observations can explain the slow kinetics of intermolecular coalescence for these ReaxFF parameterizations. At the same time the potential energy isosurfaces indicate that nucleation process may be described properly in AIREBO and ReaxFF<sub>C2013</sub>/ReaxFF<sub>CHO2016</sub> since these models demonstrate no

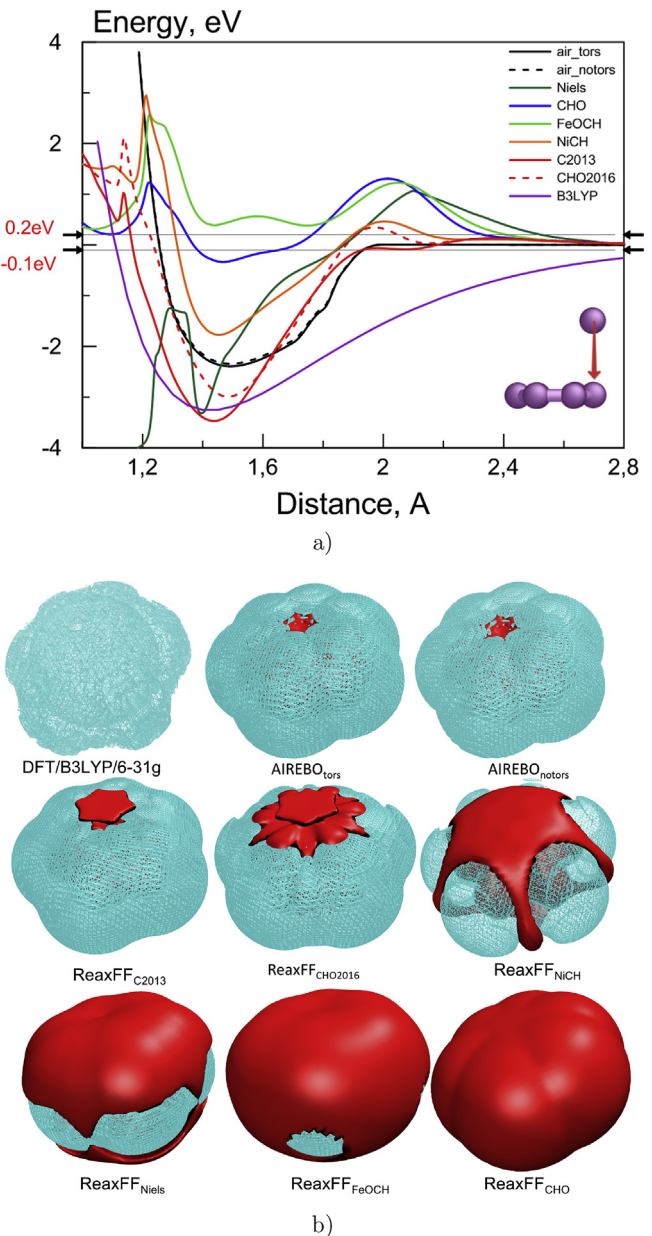


**Fig. 9.** a) The dependence of the potential energy on distance when the test atom moves perpendicular to the  $C_6$  plane. b) The interaction energy isosurfaces for a carbon hexagon and a carbon atom: the cyan surfaces show the energy  $-0.1$  eV and the red surfaces correspond to  $0.2$  eV (these barriers are shown on the plot as well). (A colour version of this figure can be viewed online.)

barriers in good agreement with the DFT. Here we should mention that there is the cutoff of covalent C–C bonds in AIREBO (2 Å), while there is no such a cutoff for much more long-ranged exponentially decaying BO-contributions in ReaxFF (e.g. sigma bonds extend up to 2.5 Å).

We should list several papers where, according to our findings, underestimation of the nucleation rate for ReaxFF<sub>CHO</sub> revealed itself. In Ref. [14] during the study of fullerene nucleation from a hydrocarbon precursor it was shown that nucleation rates for ReaxFF<sub>CHO</sub> at  $T = 2500$ K are much lower than it was expected from DFTB. Similar observations are made during comparison between ReaxFF<sub>CHO</sub> and DFTB for hydrocarbon pyrolysis at  $T = 2500 – 3500$  K [108]. This disagreement could be a result of a misleading repulsive barrier around  $sp$ -hybridized molecules for ReaxFF<sub>CHO</sub>

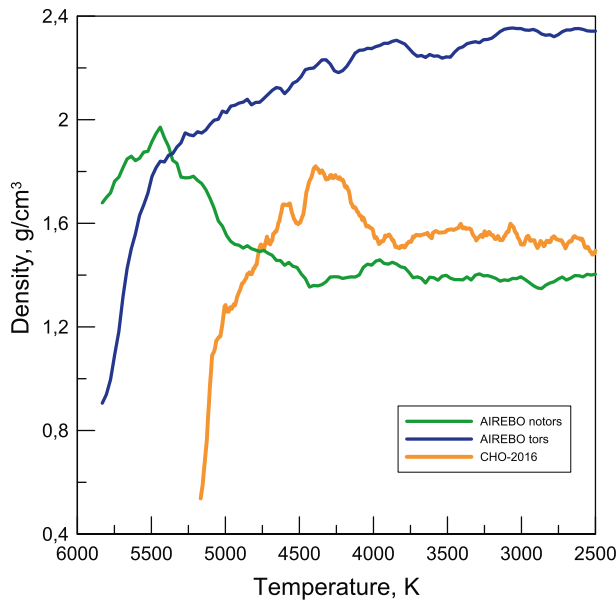


**Fig. 10.** Density of nanocluster over the cooling. (A colour version of this figure can be viewed online.)

(Fig. 9b).

#### 4.3. Torsion barrier and its influence on graphitization

It is highly surprising to observe that inclusion of small torsional barriers in AIREBO suppresses the graphitization process (Figs. 6 and 7c). While for AIREBO<sub>notors</sub> we observe almost defect-free fullerene-like nanoparticle already at  $T = 5500\text{ K}$ , AIREBO<sub>tors</sub> results in a dense low-graphitized droplet of amorphous carbon during the whole cooling procedure.

In the temperature range  $T = 5500 – 4500\text{ K}$  AIREBO<sub>tors</sub> and ReaxFF<sub>C2013</sub> systems are already arranged into a single cluster but do not form onion-like structure. They form disordered liquid or amorphous singly connected phase, therefore we are allowed to compute its density in the traditional way by simply calculating the number of atoms per volume unit. Fig. 10 demonstrates the density of the system after clusterization for ReaxFF<sub>C2013</sub>, AIREBO<sub>tors</sub> and AIREBO<sub>notors</sub> models. For ReaxFF<sub>C2013</sub> one can see two distinct trends: up to temperature  $T \approx 4400\text{ K}$  the liquid carbon is densified up to  $\rho \approx 2\text{ g/cc}$  almost reaching the bulk density of graphite, but at  $T < 4400\text{ K}$  due to fast graphitization it transforms into hollow onion-like structure with lower density. The same but less pronounced trend can be seen for AIREBO<sub>notors</sub> around  $T \approx 5500\text{ K}$ . The temperature at which we observe this kink on the density curve ( $T \approx 4400\text{ K}$  for ReaxFF<sub>C2013</sub> and  $T \approx 5500\text{ K}$  for AIREBO<sub>notors</sub>) coincides with the start of the graphitization process (see Fig. 6b and  $T_{\text{gr}}$  in Table 2). But for AIREBO<sub>tors</sub> we do not observe any non-uniformity that can be attributed to phase transition: the cluster being initially dense cools into even more dense amorphous particle.

Previously we have shown that during graphitization a carbon nanocluster demonstrates almost no change in bond length or valence angle distributions and exhibits rearrangements of dihedral angles [24]. Highly-graphitized materials consist of nearly planar, sometimes curved graphene-like elements for which dihedral angles are distributed around the values of 0 and  $180^\circ$ . It could mean that large difference between torsional angle distributions in liquid and solid phases (resulting from a rather small torsional barrier) can suppress the graphitization process.

It appears that for AIREBO such slight alteration in torsional barriers around  $sp^2-sp^2$  bonds significantly change the structure of liquid carbon. Fig. 11 demonstrates the distribution of torsion angles in liquid carbon at  $T = 5000\text{ K}$  and pressure 0.5 GPa for models considered and their difference with DFT. For DFT calculations we use a supercell containing 128 atoms and the PAW potential with four outer-shell electrons for carbon and the PBE exchange-correlation functional. The timestep is set to 0.5 fs, the cutoff energy for plane waves is 700 eV and only the gamma point in the Brillouin zone is used. Final atomic configurations from ReaxFF<sub>C2013</sub> and AIREBO<sub>tors</sub> are taken as initial atom positions for two independent calculation in VASP [109].

Fig. 11 gives possible explanation why AIREBO<sub>tors</sub> is less likely to graphitize: the overall number of dihedral angles which are needed to be rearranged is several times larger in comparison with ReaxFF<sub>C2013</sub> or DFT and such transformation requires much more acts of C–C bond breaking [24]. It means that inclusion of relatively small torsion barrier in AIREBO<sub>tors</sub> makes graphitization of carbon nanoparticle during the quenching more energetically demanding.

To investigate the nature of such drastic changes appeared after the variations of the torsion component in AIREBO we utilize the methodology discussed in Ref. [37]: we calculate the potential energy barriers for two reference molecules ( $C_6H_8$  and  $C_6H_{12}$ , see Fig. 12) for different dihedral angles, which correspond to the rotation over the central C–C bond. In the first molecule  $sp^2$  C–C bond is connected to  $sp^2$ -hybridized carbon atoms, while in the second it is connected to  $sp^3$ -hybridized atoms. It is assumed that atom's bonding environment in liquid carbon containing a certain amount of both  $sp^2$  and  $sp^3$ -hybridized atoms resembles an intermediate case between these two cases. The calculated barriers for  $C_6H_8$  are only on the order of 0.1 – 0.3 of eV (Fig. 12a). Nevertheless, all of the reactive potentials considered demonstrate poor agreement with DFT in terms of the shape of the torsional barrier: none of them reproduces the peak at  $45^\circ$  angle even qualitatively.

In Ref. [37] the authors argued that the unsaturated  $CH_2$  side groups of the  $C_6H_8$  molecule create an “embedding” for the central  $sp^2$  C–C bond that captures important aspects of  $sp^2$  bonds in liquid carbon (the effects of lone pair electrons). These lone pair electrons are responsible for the energy maximum at  $45^\circ$  in DFT calculations. On Fig. 12b we show the comparison of the AIREBO and ReaxFF results and the DFT results for the  $C_6H_{12}$  molecule (that is closer to the molecules used in the ReaxFF training) and observe a much better agreement in both qualitative and quantitative sense. Nevertheless, our findings indicate that all of the discussed potentials have problems in reproducing the properties of disordered carbon phases with significant amount of unsaturated covalent bonds (e.g.  $sp^2$ -hybridized liquid or amorphous state).

#### 5. Comparisons with experimental data

For the further validation of the reactive MD results we analyse obtained values of  $T_{\text{cluster}}$  and  $T_{\text{gr}}$  on the basis of the known experimental parameters of phase transitions in carbon materials.

Firstly, we would like to discuss the experimental studies of carbon soot thermal stability and sublimation at  $T > 3000\text{ K}$  via laser induced incandescence (LII). Sublimation of carbon soot during the heating is the process opposite to the considered here nucleation from the gas phase at cooling: if both of them are quasi-equilibrium, their characteristic temperatures should be equal, which allows us to make estimations on the value of  $T_{\text{cluster}}$  (Figs. 3 and 7a). In LII experiments thermal radiation of particles is measured after a heating with intense laser pulse [110]. It brings information on the size and concentration of carbon particles at a particular temperature and allows measuring the temperature at which sublimation of soot takes place. In general, it is not obvious

**Table 2**

Comparison of the key properties predicted by 8 reactive models (bold font shows significant deviations from reference data).

	Reference	AIR <sub>tors</sub>	AIR <sub>notors</sub>	Niels	CHO	FeOCH	NiCH	C2013	CHO2016
Maximum level of $sp^2$	89 DFTB	89	96	<b>9</b>	92	<b>22</b>	79	97	95
hybridization at $T = 3500$ K (%)									
Maximum level of graphitization (number of hexagons)	20 DFTB	35	35	<b>1</b>	33	<b>1</b>	28	34	32
Temparature of clusterization (K)	<4500 Experiment	<b>5000</b>	<b>5500</b>	4150	4100	4300	4100	<b>4750</b>	4400
Temparature of graphitization (K)	3850 DFTB	<b>3500</b>	<b>5250</b>	n/a	3750	n/a	3750	<b>4250</b>	<b>4250</b>
3D maps (Fig. 9)	DFT	+	+	-	-	-	±	+	+
Torsion angles distribution (Fig. 11)	DFT	-	+	±	±	±	+	±	+

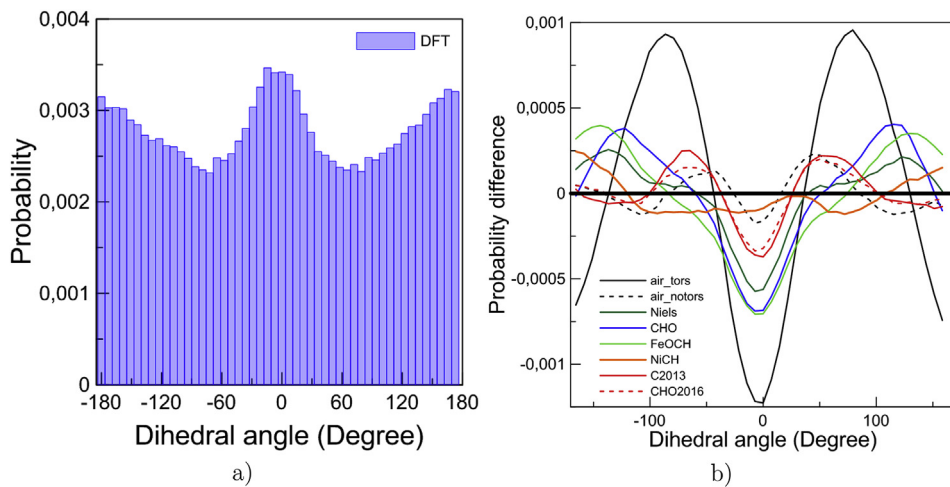


**Fig. 11.** a) The distribution of dihedral angles in liquid at  $T = 5000$  K and  $P = 0.5$  GPa calculated by DFT. b) The difference of the distributions of dihedral angles relative to DFT in liquid at  $T = 5000$  K and  $P = 0.5$  GPa. The closer the curve is to the zero line the better the reactive model reproduces the DFT results. (A colour version of this figure can be viewed online.)

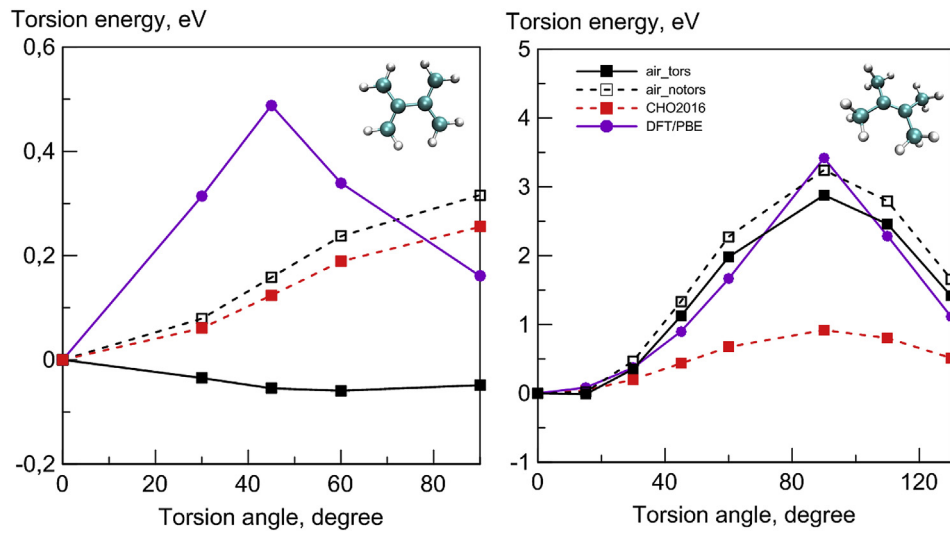


**Fig. 12.** The torsional energy as a function of torsional angle for a)  $(CH_2)_2CC(CH_2)_2$ , b)  $(CH_3)_2CC(CH_3)_2$ . (A colour version of this figure can be viewed online.)

what are the typical products of this sublimation process: depending on the soot inner structure, particle can be decomposed into  $C_2/C_3$  molecules as well as into graphene-like flakes or other fragments with much larger molecular weight [110,111]. It is expected that higher sublimation temperatures of well-annealed

particles are related to  $C_3$  and even  $C_2$  formation via intensive covalent bond breaking, while lower correspond to the breaking of weak van der Waals forces and formation of heavier products. Highest sublimation temperatures measured within such technique are located in the range  $T = 4250 – 4450$  K [99–102] (see a

dashed region on Fig. 7a).

Several recent works on the arc discharge synthesis of carbon nanoparticles provide insights on the bounds of temperature region where carbon nanoparticles formation takes place. In arc discharge experiments monoatomic carbon plasma, generated between electrodes, cools down on its way from the center of the arc forming  $C_2$  and  $C_3$  molecules which then coalescence into nanoparticles. Laser-induced fluorescence technique provides data on the spacial position and form of so-called  $C_2$  “bubble” where the first  $C_2$  dimers start to form. In Ref. [112,113] it has been shown that the approximate temperature of the  $C_2$  region is  $T > 4500\text{K}$  and subsequent carbon condensation and CNT formation starts at  $T < 4500\text{ K}$ . It gives the data less precise than LII but still quite valuable. These data support our estimation for  $T = \text{cluster } 4000\text{--}4500\text{ K}$ . In general there are no experimental evidences of carbon soot or any other condensed carbon allotropes existing at  $T > 4500\text{ K}$  and low pressures ( $P < 100\text{bar}$ ). Therefore we can conclude that clusterization temperature (Figs. 3 and 7a) should be comparable to these estimates and consider the condition  $T_{\text{cluster}} < 4500\text{ K}$  following the experimental data discussed above.

The estimation of  $T_{\text{gr}}$  based on experimental data is a bit more challenging task: in Ref. [40] we have already discussed the vast controversy of the literature data related to the analysis of graphite ( $T_{\text{melt}}^{\text{graphite}}$ ) melting temperature. Different experimental works predict different  $T_{\text{melt}}^{\text{graphite}}$  values over an extremely wide temperature range  $T_{\text{melt}}^{\text{graphite}} = 3700\text{--}6500\text{ K}$  [114–125] – for the detailed analysis of the related works see Refs. [126]). Considering the large number of experimental attempts to measure  $T_{\text{melt}}^{\text{graphite}}$ , this situation rises more likely from the misunderstanding of the physical mechanisms accompanying the graphite melting process rather than from the drawbacks of a particular experimental technique or setup. Unfortunately, sample stabilization and direct structural analysis in steady-heating experiments at  $T > 4000\text{K}$  is a challenging and still unreachable goal. For DFTB we obtain graphitization temperature  $T_{\text{gr}} \approx 3850\text{ K}$ . The lower bound of this estimation can be indirectly supported by the experimental data from Refs. [127], where it was shown that at temperature  $T = 3818\text{ K}$  and saturation vapor pressure (approximately 0.3–1 bar) graphite remains its crystal  $sp^2$ -hybridized structure on the macroscopic times. It gives us the confidence interval for the temperature of graphitization  $3850\text{ K} < T_{\text{gr}} < T_{\text{cluster}} < 4500\text{ K}$ .

The formation of multi-layered fullerenes (carbon nano-onions, CNOs) observed in this work deserves special consideration. Various techniques have been proposed for the synthesis of CNOs: the Kuznetsov method of the thermal annealing of ultradispersed nanodiamonds [128–131], electron-beam irradiation [132], carbon ion implantation into metals [133], chemical vapor deposition [134], radio-frequency plasma-enhanced chemical vapor deposition [135], arc discharge [136], arc discharge between two electrodes submerged in water [137,138] and shock-wave loading of graphite [139,140]. Onion-like structures can also appear as the co-products of CNTs damage at high pressure during the spark plasma sintering [141,142]. In the recent reviews [143,144] the CNOs production mechanisms and their possible applications were discussed.

Laser ablation of graphite and laser-induced pyrolysis in different quenching gas atmospheres [145–147] are the closest experimental analogs to the process of carbon gas condensation at rapid cooling considered in this work. In those experimental studies the formation of CNOs was observed at  $T > 4000\text{ K}$  after laser ablation of graphite and at  $T > 3500\text{ K}$  after the laser-induced pyrolysis of ethylene, acetylene and benzene vapor. Those experiments support the validity of the CNO formation mechanism

considered in this work. Another exotic experiment that can be mentioned here is the condensation of vaporized graphite inside bulk superfluid liquid helium that results in the formation of fullerene- or onion-like structures [148]: the authors argued that the similarity between such a low temperature condensation and high temperature experiments could be explained by a rise of the temperature during the condensation.

## 6. Discussion

Here we would also like to make a brief overview of the existing computational studies related to graphite and graphene melting processes. For a quasi-infinite graphene sheet located in vacuum the upper limit of graphene melting temperature  $T_{\text{melt}}^{\text{graphene}}$  for LCBOPII potential [32,33] was estimated to be  $4900\text{ K}$  [86]. Several years later the same group demonstrated that describing of graphene melting by the kinetic nucleation theory decreases  $T_{\text{melt}}^{\text{graphene}}$  down to  $4510\text{ K}$  [149]. Recently melting of quasi-infinite graphene sheet was modeled with AIREBO potential in the presence of an inert gas which gave an opportunity to vary the pressure in the computational cell [150]. In Refs. [151] melting of graphene nanoclusters was modeled on the basis of SCC-DFTB. For a cluster containing 100–200 atoms melting temperature is approximately  $4000\text{--}4100\text{K}$ , which is close to our estimation of  $T_{\text{gr}} \approx 3850\text{ K}$  for DFTB (Fig. 7c). In general, all of the computational works related to this subject demonstrate one and the same mechanism of graphene thermal decomposition: a transition from  $sp^2$ -hybridized 2D sheet to a complicated mixture of branched mostly  $sp$ -hybridized carbon chains.

It is worth mentioning that throughout all of our computations, including both DFTB and classical MD approaches, we observe  $T_{\text{gr}} < T_{\text{cluster}}$ . From the physical point of view it denotes the possibility of temperature region existence where carbon resides in liquid (or polymer-like gel, as it has been called in Ref. [86]) form at relatively low pressures [152]. According to Fig. 4 this phase is predominantly  $sp$ -hybridized. The width of this region varies depending on the chosen potential and reaches its minimal value of about  $100\text{--}200\text{ K}$  for DFTB.

It is also interesting to note that despite in [37] it was shown that incorrect torsional barriers could significantly affect the structure of liquid carbon and even resulted in the misleading observation of a liquid-liquid phase transition, recent MD studies did not incorporate any kind of dihedral angle analysis, focusing mostly on covalent bond and valence angle distributions. We show here that the inaccurate description of C–C torsion barriers could lead to major changes in rates and mechanisms of carbon nanocluster formation. Despite the fact that none of the considered carbon potentials demonstrate even qualitative agreement with DFT on the torsional barrier in a simple hydrocarbon molecule  $(CH_2)_2CC(CH_2)_2$  (Fig. 12), Reax<sub>CHO2016</sub>, Reax<sub>NiCH</sub> and AIREBO<sub>tors</sub> reproduce the torsional angle distribution in liquid carbon well (Fig. 11).

The comparison of the reactive models and their validation discussed in the present study are summarized in Table 2:

1. AIREBO<sub>tors</sub> and AIREBO<sub>notors</sub> both predict the existence of the condensed phase already at  $T = 5500\text{--}5700\text{ K}$  that contradicts the existing experimental observations.
2. For ReaxFF<sub>Niels</sub> and ReaxFF<sub>FeOCH</sub> the levels of  $sp^2$ -hybridization and graphitization for the final structures are much lower than the reference DFTB data and the results of other models.
3. ReaxFF<sub>C2013</sub> shows the clusterization and graphitization temperatures that are higher than the reference values.
4. The most optimal parametrizations among considered are ReaxFF<sub>CHO</sub>, ReaxFF<sub>NiCH</sub> and ReaxFF<sub>CHO2016</sub>. They give an

acceptable overall description of the process considered. However, the models are not free from disadvantages: ReaxFF<sub>CHO</sub> and ReaxFF<sub>NiCH</sub> shows high energy barriers that inhibit clusterization and ReaxFF<sub>CHO2016</sub> gives  $T_{gr}$  higher than the reference value.

It is necessary to mention that the descriptions presented by the authors of the parameterizations in the original papers [50–55] are not sufficient to identify the reasons of such differences.

## 7. Conclusions

All reactive MD models considered describe three main stages of structural evolution during carbon nanoparticle formation from gas phase: the clusterization, the change of hybridization in an amorphous cluster and its graphitization. Despite this qualitative similarity, the details of the corresponding MD simulations differ drastically.

On the one hand, AIREBO predicts rapid clusterization of gas into amorphous droplets already at high temperatures and rapid subsequent graphitization of these clusters. On the other hand, ReaxFF<sub>Niels</sub> and ReaxFF<sub>FeOCH</sub> models show very low graphitization even at lowest temperatures considered.

In order to validate the results of the reactive models we have used *ab initio* electronic structure calculations with DFTB and DFT that have revealed the following instructive facts:

- Three reactive models (ReaxFF<sub>Niels</sub>, ReaxFF<sub>CHO</sub>, ReaxFF<sub>FeOCH</sub>) are characterized by the repulsive energy barrier for atomic collisions with molecules that is not confirmed by DFT calculations and may inhibit the clusterization process.
- The corrections of the torsion angle energy contributions introduced in AIREBO<sub>tors</sub> can not be considered negligible as was initially assumed. These corrections make torsion angle distribution in the liquid carbon modeled with AIREBO<sub>tors</sub> unrealistic that strongly inhibits graphitization.
- Interestingly, despite the deficiencies in the description of C–C bond rotation for a single hydrocarbon molecule, all ReaxFF models adequately reproduce the torsion angle distribution in liquid carbon.
- DFTB calculations has provided an estimate of the graphitization temperature  $T_{gr} = 3850$  K that correlates reasonably with the estimates of the graphite melting temperature and serves as a reference value for reactive MD models validation.

The estimates based on the analysis of experimental data for  $T_{cluster}$  and our DFTB results for  $T_{gr}$  have given us the confidence interval  $3850\text{ K} < T_{gr} < T_{cluster} < 4500\text{ K}$ .

The validation conditions developed in this work have allowed us to select three ReaxFF models as the most optimal reactive potentials for MD modeling of the carbon nanoparticle formation. These three models, however, have certain minor drawbacks: ReaxFF<sub>CHO</sub> [51] demonstrates high energy barriers that slow down clusterization, ReaxFF<sub>NiCH</sub> [53] has excessive clusterization energy barriers as well and in cooling simulations it shows the final structure with low graphitization level, ReaxFF<sub>CHO2016</sub> [55] predicts  $T_{gr}$  about 400 K higher than the reference value. Until new better reactive models are under development, for the accurate predictive modeling we recommend using simultaneously these three models for reactive MD studies of the carbon nanoparticle formation. The subsequent comparison of the results of these MD simulations will provide much better validated predictions than the results obtained with some arbitrarily selected reactive model.

## CRedit authorship contribution statement

**Nikita Orekhov:** Conceptualization, Data curation, Investigation, Methodology, Writing – original draft, preparation. **Gulnaz Ostroumova:** Data curation, Investigation, Methodology, Validation, Visualization, Writing – original draft, preparation. **Vladimir Stegailov:** Conceptualization, Methodology, Supervision, Writing – review & editing.

## Declaration of competing interest

The authors declare that they have no known competing financial interests or personal relationships that could have appeared to influence the work reported in this paper.

## Acknowledgments

The authors gratefully acknowledge financial support from the Government of the Russian Federation (Agreement No. 074-02-2018-286) and the President grant NS-5922.2018.8. The article was prepared within the framework of the HSE University Basic Research Program.

The authors acknowledge the supercomputer centre of JIHT RAS, the supercomputer centre of MIPT and the supercomputer center of NRU HSE for the access to computational resources.

## References

- [1] W. Krätschmer, L.D. Lamb, K. Fostiropoulos, D.R. Huffman, Solid C 60: a new form of carbon, *Nature* 347 (6291) (1990) 354–358.
- [2] M.S. Dresselhaus, G. Dresselhaus, P.C. Eklund, *Science of Fullerenes and Carbon Nanotubes: Their Properties and Applications*, Elsevier, 1996.
- [3] F. Banhart, P.M. Ajayan, Carbon onions as nanoscopic pressure cells for diamond formation, *Nature* 382 (6590) (1996) 433–435.
- [4] D. Jariwala, V.K. Sangwan, L.J. Lauhon, T.J. Marks, M.C. Hersam, Carbon nanomaterials for electronics, optoelectronics, photovoltaics, and sensing, *Chem. Soc. Rev.* 42 (7) (2013) 2824–2860.
- [5] S. Li, K.V. Larionov, Z.I. Popov, T. Watanabe, K. Amemiya, S. Entani, P.V. Avramov, Y. Sakuraba, H. Naramoto, P.B. Sorokin, et al., Graphene/half-metallic Heusler alloy: a novel heterostructure toward high-performance graphene spintronic devices, *Adv. Mater.* (2019) 1905734.
- [6] A. Khabibrahmanov, P. Sorokin, Carbon on the nanoscale: ultrastiffness and unambiguous definition of incompressibility, *Carbon* 160 (2020) 228–235.
- [7] F.H. Stillinger, T.A. Weber, Computer simulation of local order in condensed phases of silicon, *Phys. Rev. B* 31 (8) (1985) 5262.
- [8] J. Tersoff, Empirical interatomic potential for carbon, with applications to amorphous carbon, *Phys. Rev. Lett.* 61 (25) (1988) 2879.
- [9] D.W. Brenner, Empirical potential for hydrocarbons for use in simulating the chemical vapor deposition of diamond films, *Phys. Rev. B* 42 (15) (1990) 9458.
- [10] V.L. Kuznetsov, A.N. Usoltseva, A.L. Chuvilin, E.D. Obraztsova, J.-M. Bonard, Thermodynamic analysis of nucleation of carbon deposits on metal particles and its implications for the growth of carbon nanotubes, *Phys. Rev. B* 64 (23) (2001) 235401.
- [11] S.A. Gubin, I.V. Maklashova, E.I. Zakatilova, Enthalpy of formation of single- and multilayer graphene, *Russ. J. Phys. Chem.* 89 (8) (2015) 1434–1438.
- [12] S. Kozlova, S. Gubin, I. Maklashova, A. Seleznev, Molecular-dynamic simulations of the thermophysical properties of hexanitrohexaazaisowurtzitane single crystal at high pressures and temperatures, *Russ. J. Phys. Chem.* 91 (11) (2017) 2157–2160.
- [13] N. Kondratyuk, D. Lenev, V. Pisarev, Transport coefficients of model lubricants up to 400 mpa from molecular dynamics, *J. Chem. Phys.* 152 (19) (2020) 191104.
- [14] H.-J. Qian, A.C. van Duin, K. Morokuma, S. Irle, Reactive molecular dynamics simulation of fullerene combustion synthesis: ReaxFF vs DFTB potentials, *J. Chem. Theor. Comput.* 7 (7) (2011) 2040–2048.
- [15] M. Shariat, S. Hosseini, B. Shokri, E. Neyts, Plasma enhanced growth of single walled carbon nanotubes at low temperature: a reactive molecular dynamics simulation, *Carbon* 65 (2013) 269–276.
- [16] B.P. Uberuaga, S.J. Stuart, W. Windl, M.P. Masquelier, A.F. Voter, Fullerene and graphene formation from carbon nanotube fragments, *Computational and Theoretical Chemistry* 987 (2012) 115–121.
- [17] N. Lümmen, Aggregation of carbon in an atmosphere of molecular hydrogen investigated by ReaxFF-molecular dynamics simulations, *Comput. Mater. Sci.* 49 (2) (2010) 243–252.
- [18] Q. Mao, A.C. van Duin, K. Luo, Formation of incipient soot particles from

- polycyclic aromatic hydrocarbons: a ReaxFF molecular dynamics study, *Carbon* 121 (2017) 380–388.
- [19] S. Han, X. Li, F. Nie, M. Zheng, X. Liu, L. Guo, Revealing the initial chemistry of soot nanoparticle formation by ReaxFF Molecular Dynamics Simulations, *Energy Fuels* 31 (8) (2017) 8434–8444.
- [20] B.D. Jensen, A. Bandyopadhyay, K.E. Wise, G.M. Odegard, Parametric study of ReaxFF simulation parameters for molecular dynamics modeling of reactive carbon gases, *J. Chem. Theor. Comput.* 8 (9) (2012) 3003–3008.
- [21] V. Dozhdikov, A.Y. Basharin, P. Levashov, D. Minakov, Atomistic simulations of the equation of state and hybridization of liquid carbon at a temperature of 6000 K in the pressure range of 1–25 GPa, *J. Chem. Phys.* 147 (21) (2017) 214302.
- [22] C. de Tomas, I. Suarez-Martinez, N.A. Marks, Graphitization of amorphous carbons: a comparative study of interatomic potentials, *Carbon* 109 (2016) 681–693.
- [23] C. de Tomas, A. Aghajamali, J.L. Jones, D.J. Lim, M.J. Lopez, I. Suarez-Martinez, N.A. Marks, Transferability in interatomic potentials for carbon, *Carbon* 155 (2019) 624–634.
- [24] G. Ostroumov, N. Orekhov, V. Stegailov, Reactive molecular-dynamics study of onion-like carbon nanoparticle formation, *Diam. Relat. Mater.* 94 (2019) 14–20.
- [25] S.J. Stuart, A.B. Tutein, J.A. Harrison, A reactive potential for hydrocarbons with intermolecular interactions, *J. Chem. Phys.* 112 (14) (2000) 6472–6486.
- [26] A.C.T. Van Duin, S. Dasgupta, F. Lorant, W.A.I. Goddard, ReaxFF: a reactive force field for hydrocarbons, *J. Phys. Chem.* 105 (41) (2001) 9396–9409.
- [27] O. Kum, F.H. Ree, S.J. Stuart, C.J. Wu, Molecular dynamics investigation on liquid–liquid phase change in carbon with empirical bond-order potentials, *J. Chem. Phys.* 119 (12) (2003) 6053–6056.
- [28] N. Marks, Generalizing the environment-dependent interaction potential for carbon, *Phys. Rev. B* 63 (3) (2000), 035401.
- [29] A.P. Bartók, M.C. Payne, R. Kondor, G. Csányi, Gaussian approximation potentials: the accuracy of quantum mechanics, without the electrons, *Phys. Rev. Lett.* 104 (13) (2010) 136403.
- [30] V.L. Deringer, G. Csányi, Machine learning based interatomic potential for amorphous carbon, *Phys. Rev. B* 95 (9) (2017), 094203.
- [31] J. Los, A. Fasolino, Intrinsic long-range bond-order potential for carbon: performance in Monte Carlo simulations of graphitization, *Phys. Rev. B* 68 (2) (2003), 024107.
- [32] J.H. Los, L.M. Ghiringhelli, E.J. Meijer, A. Fasolino, Improved long-range reactive bond-order potential for carbon, I. Construction, *Physical Review B* 72 (21) (2005) 214102.
- [33] L.M. Ghiringhelli, J.H. Los, A. Fasolino, E.J. Meijer, Improved long-range reactive bond-order potential for carbon. II. Molecular simulation of liquid carbon, *Phys. Rev. B* 72 (21) (2005) 214103.
- [34] D. Pettifor, New many-body potential for the bond order, *Phys. Rev. Lett.* 63 (22) (1989) 2480.
- [35] D. Pettifor, I. Oleinik, Analytic bond-order potentials beyond Tersoff-Brenner. I. Theory, *Phys. Rev. B* 59 (13) (1999) 8487.
- [36] I. Oleinik, D. Pettifor, Analytic bond-order potentials beyond Tersoff-Brenner. II. Application to the hydrocarbons, *Phys. Rev. B* 59 (13) (1999) 8500.
- [37] C.J. Wu, J.N. Glosli, G. Galli, F.H. Ree, Liquid–liquid phase transition in elemental carbon: a first-principles investigation, *Phys. Rev. Lett.* 89 (13) (2002) 135701.
- [38] D.W. Brenner, J.A. Harrison, C.T. White, R.J. Colton, Molecular dynamics simulations of the nanometer-scale mechanical properties of compressed Buckminsterfullerene, *Thin Solid Films* 206 (1) (1991) 220–223.
- [39] G. Dhaliwal, P.B. Nair, C.V. Singh, Uncertainty analysis and estimation of robust airebo parameters for graphene, *Carbon* 142 (2019) 300–310.
- [40] N. Orekhov, V. Stegailov, Graphite melting: atomistic kinetics bridges theory and experiment, *Carbon* 87 (2015) 358–364.
- [41] N. Orekhov, V. Stegailov, Kinetics of graphite melting, in: *Doklady Physics*, vol. 60, Springer, 2015, pp. 109–113.
- [42] N. Orekhov, V. Stegailov, Molecular-dynamics based insights into the problem of graphite melting, *J. Phys. Conf.* 653 (1) (2015), 012090.
- [43] D.W. Brenner, Erratum: empirical potential for hydrocarbons for use in simulating the chemical vapor deposition of diamond films, *Phys. Rev. B* 46 (3) (1992) 1948.
- [44] J. Hur, S.J. Stuart, Modified reactive empirical bond-order potential for heterogeneous bonding environments, *J. Chem. Phys.* 137 (5) (2012), 054102.
- [45] T.C. O'Connor, J. Andzelin, M.O. Robbins, AIREBO-M: a reactive model for hydrocarbons at extreme pressures, *J. Chem. Phys.* 142 (2) (2015), 024903.
- [46] A.F. Fonseca, G. Lee, T.L. Borders, H. Zhang, T.W. Kemper, T.-R. Shan, S.B. Sinnott, K. Cho, Reparameterization of the rebo-cho potential for graphene oxide molecular dynamics simulations, *Phys. Rev. B* 84 (7) (2011), 075460.
- [47] H. Zhao, K. Min, N. Aluru, Size and chirality dependent elastic properties of graphene nanoribbons under uniaxial tension, *Nano Lett.* 9 (8) (2009) 3012–3015.
- [48] J.A. Baimova, B. Liu, S.V. Dmitriev, N. Srikanth, K. Zhou, Mechanical properties of bulk carbon nanostructures: effect of loading and temperature, *Phys. Chem. Chem. Phys.* 16 (36) (2014) 19505–19513.
- [49] E. Iakovlev, P. Zhilyaev, I. Akhatov, Atomistic study of the solid state inside graphene nanobubbles, *Sci. Rep.* 7 (1) (2017) 1–7.
- [50] K.D. Nielson, A.C. van Duin, J. Osgaard, W.-Q. Deng, W.A. Goddard, Development of the ReaxFF reactive force field for describing transition metal catalyzed reactions, with application to the initial stages of the catalytic formation of carbon nanotubes, *J. Phys. Chem.* 109 (3) (2005) 493–499.
- [51] K. Chenoweth, A.C.T. Van Duin, W.A.I. Goddard, ReaxFF reactive force field for molecular dynamics simulations of hydrocarbon oxidation, *J. Phys. Chem.* 112 (5) (2008) 1040–1053.
- [52] M. Aryanpour, A.C. van Duin, J.D. Kubicki, Development of a reactive force field for iron- oxyhydroxide systems, *J. Phys. Chem.* 114 (21) (2010) 6298–6307.
- [53] J.E. Mueller, A.C. van Duin, W.A. Goddard III, Development and validation of ReaxFF reactive force field for hydrocarbon chemistry catalyzed by nickel, *J. Phys. Chem. C* 114 (11) (2010) 4939–4949.
- [54] S.G. Srinivasan, A.C.T. van Duin, P. Ganesh, Development of a ReaxFF potential for carbon condensed phases and its application to the thermal fragmentation of a large fullerene, *J. Phys. Chem.* 119 (4) (2015) 571–580.
- [55] C. Ashraf, A.C. van Duin, Extension of the ReaxFF combustion force field toward syngas combustion and initial oxidation kinetics, *J. Phys. Chem.* 121 (5) (2017) 1051–1068.
- [56] O.V. Sergeev, A.V. Yanilkin, Hydrogen transfer in energetic materials from ReaxFF and DFT calculations, *J. Phys. Chem.* 121 (16) (2017) 3019–3027.
- [57] T.P. Senftle, S. Hong, M.M. Islam, S.B. Kylasa, Y. Zheng, Y.K. Shin, C. Junkermeier, R. Engel-Herbert, M.J. Janik, H.M. Aktulga, et al., The ReaxFF reactive force-field: development, applications and future directions, *npj Computational Materials* 2 (2016) 15011.
- [58] K. Krylova, Y.A. Baimova, S. Dmitriev, R. Mulyukov, Calculation of the structure of carbon clusters based on fullerene-like C<sub>24</sub> and C<sub>48</sub> molecules, *Phys. Solid State* 58 (2) (2016) 394–401.
- [59] R. Ranganathan, S. Rokkam, T. Desai, P. Kebbinski, Generation of amorphous carbon models using liquid quench method: a reactive molecular dynamics study, *Carbon* 113 (2017) 87–99.
- [60] S. Winczewski, M.Y. Shaheen, J. Rybicki, Interatomic potential suitable for the modeling of penta-graphene: molecular statics/molecular dynamics studies, *Carbon* 126 (2018) 165–175.
- [61] H. Su, R.J. Nielsen, A.C.T. van Duin, W.A. Goddard III, Simulations on the effects of confinement and Ni-catalysis on the formation of tubular fullerene structures from peapod precursors, *Phys. Rev. B* 75 (2007) 134107.
- [62] N. Lummen, ReaxFF-molecular dynamics simulations of non-oxidative and non-catalyzed thermal decomposition of methane at high temperatures, *Phys. Chem. Chem. Phys.* 12 (2010) 7883–7893.
- [63] H. Zhan, G. Zhang, Y. Zhang, V. Tan, J.M. Bell, Y. Gu, Thermal conductivity of a new carbon nanotube analog: the diamond nanothread, *Carbon* 98 (2016) 232–237.
- [64] T. Botari, R. Paupitz, P.A. da Silva Autreto, D.S. Galvao, Graphene healing mechanisms: a theoretical investigation, *Carbon* 99 (2016) 302–309.
- [65] K. Li, H. Zhang, G. Li, J. Zhang, M. Bouhadja, Z. Liu, A.A. Skelton, M. Barati, ReaxFF molecular dynamics simulation for the graphitization of amorphous carbon: a parametric study, *J. Chem. Theor. Comput.* 14 (5) (2018) 2322–2331.
- [66] R. Subbaraman, S.A. Deshmukh, S.K. Sankaranarayanan, Atomistic insights into early stage oxidation and nanoscale oxide growth on Fe (100), Fe (111) and Fe (110) surfaces, *J. Phys. Chem. C* 117 (10) (2013) 5195–5207.
- [67] G. Galiullina, N. Orekhov, V. Stegailov, Nucleation of carbon nanostructures: molecular dynamics with reactive potentials, *J. Phys. Conf.* 774 (1) (2016), 012033.
- [68] G. Galiullina, N. Orekhov, V. Stegailov, Nanostructures nucleation in carbon–metal gaseous phase: a molecular dynamics study, *J. Phys. Conf.* 946 (1) (2018), 012110.
- [69] M. Zarshenas, K. Moshkunov, B. Czerwinski, T. Leyssens, A. Delcorte, Molecular dynamics simulations of hydrocarbon film growth from acetylene monomers and radicals: effect of substrate temperature, *J. Phys. Chem. C* 122 (27) (2018) 15252–15263.
- [70] U. Khalilov, A. Bogaerts, E.C. Neyts, Atomic-scale mechanisms of plasma-assisted elimination of nascent base-grown carbon nanotubes, *Carbon* 118 (2017) 452–457.
- [71] J.A. Elliott, Y. Shibuta, H. Amara, C. Bichara, E.C. Neyts, Atomistic modelling of CVD synthesis of carbon nanotubes and graphene, *Nanoscale* 5 (15) (2013) 6662–6676.
- [72] E. Neyts, A. Bogaerts, Ion irradiation for improved graphene network formation in carbon nanotube growth, *Carbon* 77 (2014) 790–795.
- [73] E.C. Neyts, Y. Shibuta, A.C.T. van Duin, A. Bogaerts, Catalyzed growth of carbon nanotube with definable chirality by hybrid molecular dynamics-force biased Monte Carlo simulations, *ACS Nano* 4 (11) (2010) 6665–6672.
- [74] U. Khalilov, A. Bogaerts, E.C. Neyts, Atomic scale simulation of carbon nanotube nucleation from hydrocarbon precursors, *Nat. Commun.* 6 (2015) 10306.
- [75] H. Zhao, Q. Shi, Z. Han, H. Gong, Z. Zhang, S. Wu, J. Wu, Anomalous thermal stability in supergiant onion-like carbon fullerenes, *Carbon* 138 (2018) 243–256.
- [76] R. Ranganathan, S. Rokkam, T. Desai, P. Kebbinski, Generation of amorphous carbon models using liquid quench method: a reactive molecular dynamics study, *Carbon* 113 (2017) 87–99.
- [77] J.W. Martin, G.J. McIntosh, R. Arul, R.N. Oosterbeek, M. Kraft, T. Söhnela, Giant fullerene formation through thermal treatment of fullerene soot, *Carbon* 125 (2017) 132–138.
- [78] J. Huang, F. Ding, K. Jiao, B.I. Yakobson, Real time microscopy, kinetics, and mechanism of giant fullerene evaporation, *Phys. Rev. Lett.* 99 (17) (2007)

- 175503.
- [79] URL, <https://github.com/lammps/lammps/issues/59>.
- [80] P. Plimpton, and S. Crozier, A. Thompson, LAMMPS-large-scale atomic/molecular massively parallel simulator, Sandia National Laboratories 18.
- [81] S. Nose, A molecular dynamics method for simulations in the canonical ensemble, *Mol. Phys.* 52 (2) (1984) 255–268.
- [82] S. Maruyama, Y. Yamaguchi, A molecular dynamics demonstration of annealing to a perfect C<sub>60</sub> structure, *Chem. Phys. Lett.* 286 (3–4) (1998) 343–349.
- [83] Y. Yamaguchi, S. Maruyama, A molecular dynamics simulation of the fullerene formation process, *Chem. Phys. Lett.* 286 (3–4) (1998) 336–342.
- [84] X. Fang, A. Shashurin, G. Teel, M. Keidar, Determining synthesis region of the single wall carbon nanotubes in arc plasma volume, *Carbon* 107 (2016) 273–280.
- [85] B. Li, Y. Nan, P. Zhang, X. Song, Reducing dimensions of nanocarbons in electric arc plasma via rapid flow treatment, *Diam. Relat. Mater.* 73 (2017) 148–153.
- [86] K.V. Zakharchenko, A. Fasolino, J. Los, M. Katsnelson, Melting of graphene: from two to one dimension, *J. Phys. Condens. Matter* 23 (20) (2011) 202202.
- [87] F. Pietrucci, W. Andreoni, Fate of a graphene flake: a new route toward fullerenes disclosed with ab initio simulations, *J. Chem. Theor. Comput.* 10 (3) (2014) 913–917.
- [88] J.C. Palmer, K.E. Gubbins, Atomistic models for disordered nanoporous carbons using reactive force fields, *Microporous Mesoporous Mater.* 154 (2012) 24–37.
- [89] R. Andrews, D. Jacques, D. Qian, E. Dickey, Purification and structural annealing of multiwalled carbon nanotubes at graphitization temperatures, *Carbon* 39 (11) (2001) 1681–1687.
- [90] B. Saha, S. Shindo, S. Irle, K. Morokuma, Quantum chemical molecular dynamics simulations of dynamic fullerene self-assembly in benzene combustion, *ACS Nano* 3 (8) (2009) 2241–2257.
- [91] B. Saha, S. Irle, K. Morokuma, Hot giant fullerenes eject and capture C<sub>2</sub> molecules: QM/MD simulations with constant density, *J. Phys. Chem. C* 115 (46) (2011) 22707–22716.
- [92] S. Irle, A.J. Page, B. Saha, Y. Wang, K.R.S. Chandrakumar, Y. Nishimoto, H.-J. Qian, K. Morokuma, Atomistic mechanism of carbon nanostructure self-assembly as predicted by nonequilibrium QM/MD simulations, in: *Practical Aspects of Computational Chemistry II*, Springer, 2012, pp. 103–172.
- [93] V.V. Stegailov, N.D. Orekhov, G.S. Smirnov, Ch. HPC hardware efficiency for quantum and classical molecular dynamics, in: *Parallel Computing Technologies: 13th International Conference*, Springer International Publishing, Cham, 2015, pp. 469–473.
- [94] D. Porezag, T. Frauenheim, T. Köhler, G. Seifert, R. Kaschner, Construction of tight-binding-like potentials on the basis of density-functional theory: application to carbon, *Phys. Rev. B* 51 (19) (1995) 12947.
- [95] S. Irle, G. Zheng, Z. Wang, K. Morokuma, Theory–experiment relationship of the “shrinking hot giant” road of dynamic fullerene self-assembly in hot carbon vapor, *Nano* 2 (2007) 21–30, 01.
- [96] G. Zheng, S. Irle, K. Morokuma, Performance of the DFTB method in comparison to DFT and semiempirical methods for geometries and energies of C<sub>20</sub>–C<sub>86</sub> fullerene isomers, *Chem. Phys. Lett.* 412 (1–3) (2005) 210–216.
- [97] J. VandeVondele, M. Krack, F. Mohamed, M. Parrinello, T. Chassaing, J. Hutter, Quickstep: fast and accurate density functional calculations using a mixed Gaussian and plane waves approach, *Comput. Phys. Commun.* 167 (2) (2005) 103–128.
- [98] C. Köhler, T. Frauenheim, Molecular dynamics simulations of CF<sub>x</sub> (x= 2, 3) molecules at Si<sub>3</sub>N<sub>4</sub> and SiO<sub>2</sub> surfaces, *Surf. Sci.* 600 (2) (2006) 453–460.
- [99] J.P. Abrahamson, M. Singh, J.P. Mathews, R.L. Vander Wal, Pulsed laser annealing of carbon black, *Carbon* 124 (2017) 380–390.
- [100] H.A. Michelsen, P.E. Schrader, F. Goulay, Wavelength and temperature dependences of the absorption and scattering cross sections of soot, *Carbon* 48 (8) (2010) 2175–2191.
- [101] E.V. Gurentsov, A.V. Eremin, E.Y. Mikheyeva, Study of thermodynamic properties of carbon nanoparticles by the laser heating method, *High Temp.* 55 (5) (2017) 723–730.
- [102] S. Schraml, S. Dankers, K. Bader, S. Will, A. Leipertz, Soot temperature measurements and implications for time-resolved laser-induced incandescence (tire-lii), *Combust. Flame* 120 (4) (2000) 439–450.
- [103] I.S. Ufimtsev, T.J. Martinez, Quantum chemistry on graphical processing units. 3. Analytical energy gradients, geometry optimization, and first principles molecular dynamics, *J. Chem. Theor. Comput.* 5 (10) (2009) 2619–2628.
- [104] A.V. Titov, I.S. Ufimtsev, N. Luehr, T.J. Martinez, Generating efficient quantum chemistry codes for novel architectures, *J. Chem. Theor. Comput.* 9 (1) (2012) 213–221.
- [105] A.D. Becke, Density-functional thermochemistry. III. The role of exact exchange, *J. Chem. Phys.* 98 (7) (1993) 5648–5652.
- [106] C. Lee, W. Yang, R.G. Parr, Development of the Colle-Salvetti correlation-energy formula into a functional of the electron density, *Phys. Rev. B* 37 (2) (1988) 785.
- [107] P. Stephens, F. Devlin, C. Chabalowski, M.J. Frisch, Ab initio calculation of vibrational absorption and circular dichroism spectra using density functional force fields, *J. Phys. Chem.* 98 (45) (1994) 11623–11627.
- [108] C.W. Bauschlicher Jr., T. Qi, E.J. Reed, A. Lenfant, J.W. Lawson, T.G. Desai, Comparison of ReaxFF, DFTB, and DFT for phenolic pyrolysis. 2. Elementary reaction paths, *J. Phys. Chem.* 117 (44) (2013) 11126–11135.
- [109] G. Kresse, J. Furthmüller, Efficient iterative schemes for ab initio total-energy calculations using a plane-wave basis set, *Phys. Rev. B* 54 (16) (1996) 11169.
- [110] H. Michelsen, C. Schulz, G. Smallwood, S. Will, Laser-induced incandescence: particulate diagnostics for combustion, atmospheric, and industrial applications, *Prog. Energy Combust. Sci.* 51 (2015) 2–48.
- [111] M.B. Shavelkina, R. Amirov, Direct synthesis of hydrogenated graphene via hydrocarbon decomposition in plasmas, *Nanosystems: Physics, Chemistry, Mathematics* 10 (1) (2019) 102–106.
- [112] V. Vekselman, A. Khrabry, I. Kaganovich, B. Stratton, R. Selinsky, Y. Raitses, Quantitative imaging of carbon dimer precursor for nanomaterial synthesis in the carbon arc, *Plasma Sources Sci. Technol.* 27 (2) (2018), 025008.
- [113] S. Yatom, A. Khrabry, J. Mitrani, A. Khodak, I. Kaganovich, V. Vekselman, B. Stratton, Y. Raitses, Synthesis of nanoparticles in carbon arc: measurements and modeling, *MRS Communications* 8 (3) (2018) 842–849.
- [114] G.J. Schoessow, Graphite triple point and solidus-liquidus interface experimentally determined up to 1000 atm, *Phys. Rev. Lett.* 21 (11) (1968) 738.
- [115] N. Gokcen, E. Chang, T. Poston, D. Spencer, Determination of graphite-liquid-vapor triple point by laser heating, *Tech. rep.*, DTIC Document, 1976. Report number SAMSO-TR-76-29.
- [116] M. Sheindlin, V. Senchenko, Experimental investigation of graphite thermodynamic properties in the vicinity of melting point, *Dokl. Akad. Nauk SSSR* 298 (6) (1988) 1383–1386.
- [117] A. Baitin, A. Lebedev, S. Romanenko, V. Senchenko, M. Sheindlin, The melting point and optical properties of solid and liquid carbon at pressures of up to 2 kbar, *High Temperatures, High Pressures* 22 (2) (1990) 157–170.
- [118] A. Cezairliyan, A. Müller, Measurement of the radiance temperature (at 655 nm) of melting graphite near its triple point by a pulse-heating technique, *Int. J. Thermophys.* 11 (4) (1990) 643–651.
- [119] G. Pottlacher, R. Hixson, S. Melnitzky, E. Kaschnitz, M. Winkler, H. Jäger, Thermophysical properties of POCO AXF-5Q graphite up to melting, *Thermochim. Acta* 218 (1993) 183–193.
- [120] E. Asinovskii, A. Kirillin, A. Kostanovskii, V. Fortov, Melting parameters of carbon, *High Temp.* 36 (5) (1998) 716–721.
- [121] M. Musella, C. Ronchi, M. Brykin, M. Sheindlin, The molten state of graphite: an experimental study, *J. Appl. Phys.* 84 (5) (1998) 2530.
- [122] V. Korobenko, A. Savvatimskiy, Blackbody design for high temperature (1800 to 5500 K) of metals and carbon in liquid states under fast heating, in: *AIP Conference Proceedings*, vol. 684, AIP Publishing, 2003, pp. 783–788.
- [123] A.Y. Basharin, M.V. Brykin, M.Y. Marin, I.S. Pakhomov, S.F. Sitnikov, Methods of increasing the measurement accuracy during the experimental determination of the melting point of graphite, *High Temp.* 42 (1) (2004) 60–67.
- [124] A. Kondratyev, A. Rakhel, Melting line of graphite, *Phys. Rev. Lett.* 122 (17) (2019) 175702.
- [125] V. Polishchuk, I. Samoilov, R.K. Amirov, A. Kirillin, V. Kiselev, Graphite melting at “low” temperature, *High Temp.* 58 (2) (2020) 197–212.
- [126] A. Savvatimskiy, Measurements of the melting point of graphite and the properties of liquid carbon (a review for 1963–2003), *Carbon* 43 (6) (2005) 1115–1142.
- [127] L. Buchnev, A. Smyslov, I. Dmitriev, A. Kuteinikov, V.I. Kostikov, Experimental-study of the enthalpy of a quasi-single crystal of graphite and glass-carbon in the temperature-range 300–3800-degrees-K, *Teplofiz. Vysok. Temp.* 25 (6) (1987) 1120–1125.
- [128] V.L. Kuznetsov, A.L. Chuvalin, Y.V. Butenko, I.Y. Mal'kov, V.M. Titov, Onion-like carbon from ultra-disperse diamond, *Chem. Phys. Lett.* 222 (4) (1994) 343–348.
- [129] L. Hawalek, A. Brodka, S. Tomita, J. Dore, V. Honkimäki, A. Burian, Transformation of nano-diamonds to carbon nano-onions studied by X-ray diffraction and molecular dynamics, *Diam. Relat. Mater.* 20 (10) (2011) 1333–1339.
- [130] M. Zeiger, N. Jäckel, M. Aslan, D. Weingarth, V. Presser, Understanding structure and porosity of nanodiamond-derived carbon onions, *Carbon* 84 (2015) 584–598.
- [131] M.Y. Popov, V.D. Churkin, B.A. Kulnitskiy, A.N. Kirichenko, K.M. Bulatov, A.A. Bykov, P.V. Zinin, V. Blank, Transformation of diamond to fullerene-type onions at pressure 70 GPa and temperature 2400 K, *Nanotechnology* 31 (31) (2020) 315602.
- [132] B. Xu, S.-I. Tanaka, Formation of giant onion-like fullerenes under Al nanoparticles by electron irradiation, *Acta Mater.* 46 (15) (1998) 5249–5257.
- [133] T. Cabioch, M. Jaouen, E. Thune, P. Guerin, C. Fayoux, M. Denanot, Carbon onions formation by high-dose carbon ion implantation into copper and silver, *Surf. Coatings. Technol.* 128 (2000) 43–50.
- [134] J. Kang, J. Li, X. Du, C. Shi, N. Zhao, P. Nash, Synthesis of carbon nanotubes and carbon onions by CVD using a Ni/Y catalyst supported on copper, *Mater. Sci. Eng., A* 475 (1–2) (2008) 136–140.
- [135] X. Chen, F. Deng, J. Wang, H. Yang, G. Wu, X. Zhang, J. Peng, W. Li, New method of carbon onion growth by radio-frequency plasma-enhanced chemical vapor deposition, *Chem. Phys. Lett.* 336 (3–4) (2001) 201–204.
- [136] X. Wang, B. Xu, X. Liu, H. Jia, I. Hideki, The Raman spectrum of nanostructured onion-like fullerenes, *Phys. B Condens. Matter* 357 (3–4) (2005) 277–281.
- [137] N. Sano, H. Wang, M. Chhowalla, I. Alexandrou, G. Amarantunga, Synthesis of carbon ‘onions’ in water, *Nature* 414 (6863) (2001) 506–507.
- [138] N. Sano, H. Wang, I. Alexandrou, M. Chhowalla, K. Teo, G. Amarantunga, K. Iimura, Properties of carbon onions produced by an arc discharge in water,

- J. Appl. Phys. 92 (5) (2002) 2783–2788.
- [139] V. Blank, V. Denisov, A. Kirichenko, B. Kulnitskiy, S.Y. Martushov, B. Mavrin, I. Perezhogin, High pressure transformation of single-crystal graphite to form molecular carbon–onions, *Nanotechnology* 18 (34) (2007) 345601.
- [140] V.D. Blank, V.D. Churkin, B.A. Kulnitskiy, I.A. Perezhogin, A.N. Kirichenko, S.V. Erohin, P.B. Sorokin, M.Y. Popov, Pressure-induced transformation of graphite and diamond to onions, *Crystals* 8 (2) (2018) 68.
- [141] E. Suslova, S. Savilov, A. Egorov, A. Shumyatsev, V. Lunin, Carbon nanotube frameworks by spark plasma sintering, *Microporous Mesoporous Mater.* 293 (2020) 109807.
- [142] E. Suslova, S. Chernyak, S. Maksimov, S. Savilov, Thermophysical features of carbon nanotubes formation by spark plasma sintering, *Carbon*.
- [143] O. Mykhailiv, H. Zubyk, M.E. Plonska-Brzezinska, Carbon nano-onions: unique carbon nanostructures with fascinating properties and their potential applications, *Inorg. Chim. Acta* 468 (2017) 49–66.
- [144] M.E. Plonska-Brzezinska, Carbon nano-onions: a review of recent progress in synthesis and applications, *ChemNanoMat* 5 (5) (2019) 568–580.
- [145] C. Jäger, H. Mutschke, T. Henning, F. Huisken, Spectral properties of gas-phase condensed fullerene-like carbon nanoparticles from far-ultraviolet to infrared wavelengths, *Astrophys. J.* 689 (1) (2008) 249.
- [146] F. Huisken, C. Jäger, H. Mutschke, T. Henning, Gas-phase condensation of nanometer-and subnanometer-sized carbon grains and polycyclic aromatic hydrocarbons, *Diam. Relat. Mater.* 18 (2–3) (2009) 392–395.
- [147] C. Jäger, F. Huisken, H. Mutschke, I.L. Jansa, T. Henning, Formation of polycyclic aromatic hydrocarbons and carbonaceous solids in gas-phase condensation experiments, *Astrophys. J.* 696 (1) (2009) 706.
- [148] S. Krasnokutski, M. Goulart, E. Gordon, A. Ritsch, C. Jäger, M. Rastogi, W. Salvenmoser, T. Henning, P. Scheier, Low-temperature condensation of carbon, *Astrophys. J.* 847 (2) (2017) 89.
- [149] J. Los, K. Zakharchenko, M. Katnelson, A. Fasolino, Melting temperature of graphene, *Phys. Rev. B* 91 (4) (2015), 045415.
- [150] Y.D. Fomin, V. Brazhkin, Comparative study of melting of graphite and graphene, *Carbon* 157 (2020) 767–778.
- [151] S.K. Singh, M. Neek-Amal, F. Peeters, Melting of graphene clusters, *Phys. Rev. B* 87 (13) (2013) 134103.
- [152] S.I. Kudryashov, A.A. Karabutov, N.B. Zorov, Thermodynamic state of the laser-induced liquid phase and position of the triple point of carbon, *Mendeleev Commun.* 8 (4) (1998) 151–152.